ADVANCED MATERIALS
www.advmat.de

Work Function-Guided Electrocatalyst Design

Zhijie Chen, Tianyi Ma, Wei Wei, Wai-Yeung Wong, Chuan Zhao, and Bing-Jie Ni**

The development of high-performance electrocatalysts for energy conversion reactions is crucial for advancing global energy sustainability. The design of catalysts based on their electronic properties (e.g., work function) has gained significant attention recently. Although numerous reviews on electrocatalysis have been provided, no such reports on work function-guided electrocatalyst design are available. Herein, a comprehensive summary of the latest advancements in work function-guided electrocatalyst design for diverse electrochemical energy applications is provided. This includes the development of work function-based catalytic activity descriptors, and the design of both monolithic and heterostructural catalysts. The measurement of work function is first discussed and the applications of work function-based catalytic activity descriptors for various reactions are fully analyzed. Subsequently, the work function-regulated material-electrolyte interfacial electron transfer (IET) is employed for monolithic catalyst design, and methods for regulating the work function and optimizing the catalytic performance of catalysts are discussed. In addition, key strategies for tuning the work function-governed material-material IET in heterostructural catalyst design are examined. Finally, perspectives on work function determination, work function-based activity descriptors, and catalyst design are put forward to guide future research. This work paves the way to the work function-guided rational design of efficient electrocatalysts for sustainable energy applications.

1. Introduction

Electrochemical energy processes show promise of sustainable energy development. Electrochemistry-driven small molecule conversion reactions, such as oxygen reduction reaction (ORR), hydrogen evolution reaction (HER), nitrogen reduction reaction (NRR), carbon dioxide reduction reaction (CO_2RR), nitrate reduction reaction (NO_3RR), urea oxidation reaction (UOR), and oxygen evolution reaction (OER) have garnered souring interest.[1] The efficiency of these reactions is largely determined by electrocatalysts which can help reduce the reaction energy barriers, accelerate the reaction kinetics, and optimize the reaction selectivity.[2] Designing high-performance catalysts thus becomes an urgent mission. Currently, descriptor-based approaches have exhibited powerful potential for accelerating the design of efficient electrocatalysts. Descriptors (e.g., *d* band center,[3] work function,[2a,4] metal e_g filling[5]) that correlate the catalytic performance of materials with the intrinsic property (mainly electronic properties) are widely used to assist high-performance catalyst development, illustrate catalytic performance, and predict the catalytic activity of novel catalysts.

Work function is defined as the minimum energy needed for removing an electron from the surface of solid materials.[6] Therefore, the work function of materials governs the interface electron transfer efficiency, which is of high importance in electrocatalysis. To date, the work function of electrocatalysts has

Z. Chen, B.-J. Ni
School of Civil and Environmental Engineering
The University of New South Wales
Sydney, NSW 2052, Australia
E-mail: bingjie.ni1@unsw.edu.au

T. Ma
School of Science
RMIT University
Melbourne, VIC 3000, Australia

W. Wei
Centre for Technology in Water and Wastewater
School of Civil and Environmental Engineering
University of Technology Sydney
Sydney, NSW 2007, Australia

W.-Y. Wong
Department of Applied Biology and Chemical Technology and Research Institute for Smart Energy
The Hong Kong Polytechnic University
Hung Hom Kowloon, Hong Kong P. R. China
E-mail: wai-yeung.wong@polyu.edu.hk

C. Zhao
School of Chemistry
The University of New South Wales
Sydney, NSW 2052, Australia

The ORCID identification number(s) for the author(s) of this article can be found under https://doi.org/10.1002/adma.202401568

DOI: 10.1002/adma.202401568

been used as a catalytic activity descriptor for diverse reactions, such as HER, OER, ORR, and CO_2RR. For instance, starting from the Pt benchmark, a decreased work function contributes to a stronger adsorption ability of H on a series of *d*-metals,[7] resulting in worse HER performance. By analyzing the work function-governed material-electrolyte interfacial electron transfer (IET), studies have illustrated the work function-reaction intermediate/reactant adsorption-catalytic performance. The use of work function-based activity descriptors has greatly aided in the development of electrocatalysts.

The work function-mediated material-electrolyte IET can be directly applied to monolithic catalyst design. Monolithic catalysts mentioned in this review refer to those catalysts designed with the work function-regulated material-electrolyte IET, no matter the phase composition of catalysts (monophase or multiphase). By regulating the work function value of materials, it is sensible to optimize the catalytic performance. Since the work function of materials is highly sensitive to their physicochemical properties (e.g., chemical composition, shape, surface termination, and size), many methods have been developed to tune the work function of materials, such as heteroatom doping,[8] vacancy engineering,[9] strain engineering,[10] component regulation,[11] nanostructure control,[12] and composite construction.[13] For example, the V dopant (5% doping level) can reduce the work function of MoS_2 from 5.5 to 5.29 eV, leading to enhanced HER performance.[14] These methods are capable of adjusting the work function of monolithic catalysts and optimizing the adsorption of reaction intermediates/reactants, thus improving the catalytic performance.

Heterostructures that combine two or more phases attract great interest for their high catalytic performance.[15] The work function of different components impacts the electronic interaction at the interface, thereby influencing the electronic properties of the resulting heterostructures.[16] Thus, the IET between different components in the heterojunction, namely the material-material IET, is highly important for work function-guided heterostructure design. Aiming at enhancing the catalytic performance of heterostructures via regulating the material-material IET, studies have focused on constructing Mott–Schottky heterojunctions[17] and Ohmic contact heterojunctions,[18] regulating work function difference,[19] designing in-plane heterostructures,[20] nanostructure control,[21] etc. By selecting materials with suitable work functions to form heterojunctions or regulating the work function of involved components in heterojunctions, the design philosophy of heterostructures focuses on optimizing the electron transfer properties at the material-material interface.

Electrocatalyst design has attracted great interest from chemists, materials scientists, and engineers due to the rapid development of electrochemistry-driven energy techniques. To date, many reviews have summarized catalyst design methodologies, based on catalytic activity descriptors.[22] Most of current reviews mainly focuses on *d* band theory,[22–23] *p* band theory,[22,23d,e,24] coordination number,[23b,d,25] binding energy,[23d,f-h,26] and e_g filling.[22,23d-f,24] Despite several papers have briefly mentioned the role of work function in designing heterostructural catalysts[23h,27] and HER catalysts,[26b] the development of work function-based activity descriptors for diverse reactions and the wide applications of work function-regulated material-electrolyte IET and material-material IET in designing efficient catalysts has not been comprehensively analyzed yet.

Herein, the current achievements in work function-guided electrocatalyst design are systematically reviewed for the first time, including the development of work function-based catalytic activity descriptors, monolithic catalyst design, as well as heterostructure design (**Figure 1**). The measurement of work function is introduced, which is followed by the application of work function-based catalytic activity descriptors for different reactions. Then, a series of methods are introduced for regulating the work function in monolithic catalyst design. Afterward, strategies for tuning the work function-governed interface electron transfer between different components for heterostructure design are analyzed. Perspectives in this field are pointed out for guiding future studies.

2. Work Function: Definition and Measurement

Work function (Φ) is defined as the minimum energy required to remove an electron from a solid material to a point just outside the solid surface.[6a] From the perspective of band structure of materials, the work function is determined as the difference in electrostatic potential for an electron between the vacuum level (E_{VAC}) and Fermi level (E_F), as depicted in **Figure 2a**. For semiconductors, the E_F generally lies between the valence band (E_V) and the conduction band (E_C), and the work function changes with physicochemical properties, such as chemical composition, crystal structure, nanostructure, and surface termination, and geometry.[28]

To experimentally determine the work function of materials, a series of methods have been developed based on various physical principles like photoelectric emission, field emission, thermionic emission, and contact potential difference. When electrons are available at the Fermi level, electrons can be excited with the former three methods for electron excitation, and the absolute value of the work function can be determined. However, there are almost no electrons at the Fermi level of semiconductors or insulators, and an indirect method that utilizes the contact potential difference is generally applied for measuring the relative values of work functions. The comparison of various methods is presented in **Table 1**.

Photoelectric emission happens when the energy of irradiated photons is higher than that of the materials' work function. The minimum photon energy needed for liberating electrons from materials or the energy of emitted electrons with zero kinetic energy (concerning E_F) can provide the work function value. For the former principle, work functions are obtained based on the relationship between photoemission current and excited photon energy, with the photoelectron emission yield spectroscopy. In terms of the latter principle, it is essential to measure the emitted electron energy. The threshold energy of the emitted electrons with zero kinetic energy is named the secondary electron cutoff, which can be tested by UPS, *etc*. Of note, the latter method represents one of the most popular strategies for calculating the work functions of electrocatalysts. For example, UPS has been used to test the cutoff energy (E_{cutoff}) and E_F of Pt@N-X-CNC (X = 0.5, 1, 2) electrocatalysts (Figure 2b).[30] According to the equation ($\Phi = h\nu - |E_{cutoff} - E_F|$), work functions of Pt@N-2-CNC, Pt@N-1-CNC,

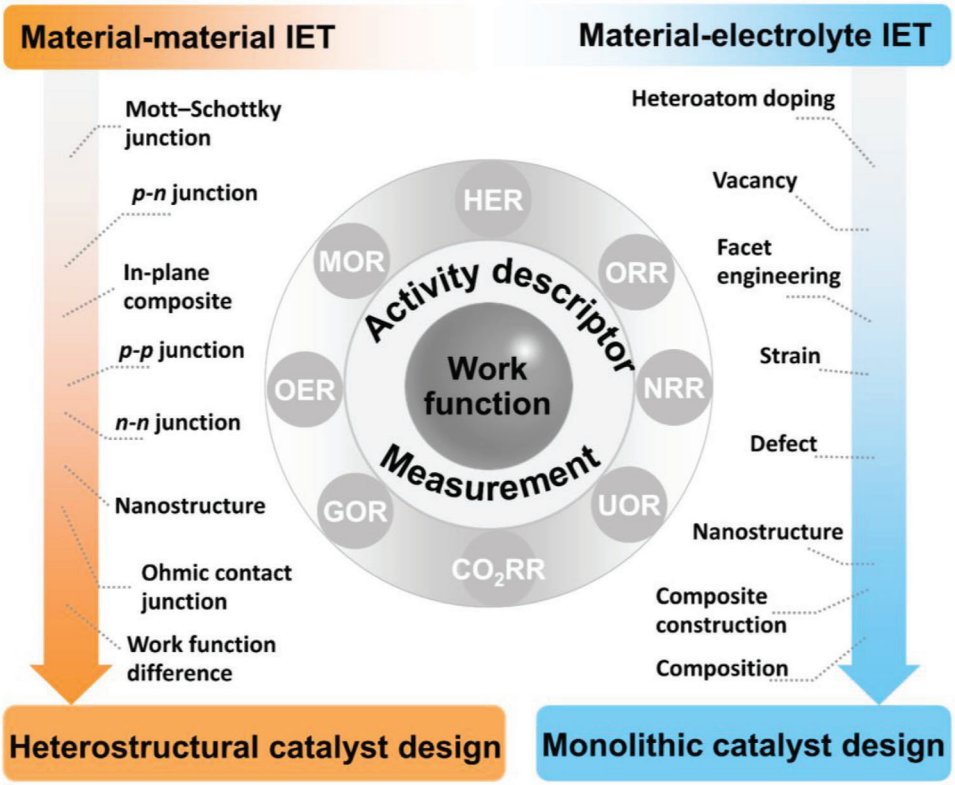

Figure 1. Scheme of the work function-guided electrocatalyst design. IET, interfacial electron transfer.

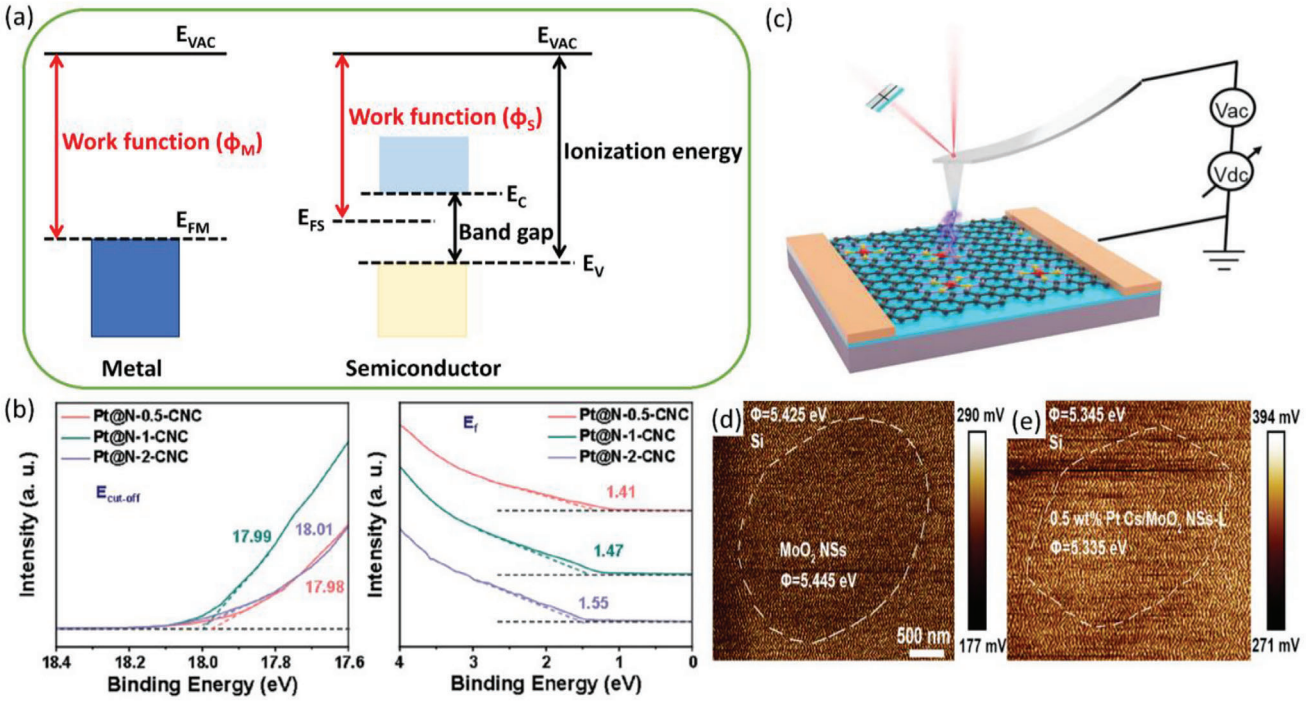

Figure 2. a) Energy diagrams of work function on the metal and the semiconductor. E_{VAC}: vacuum level, E_V: valence band maximum, E_C: conduction band minimum, E_{FM}: Fermi level of metal, and E_{FS}: Fermi level of semiconductor. b) UPS spectra of Pt@N-X-CNC (X = 0.5, 1, 2). Reprinted with permission.[30] Copyright 2023, Wiley-VCH. c) Illustration of Kelvin probe force microscopy device. V_{AC}: alternating current voltage, V_{DC}: direct current voltage. Reprinted with permission.[4] Copyright 2022, American Chemical Society. Potential images and corresponding work functions of d) MoO_2 NSs and e) 0.5 wt% Pt Cs/MoO_2 NSs-L, tested by KPFM. Reprinted with permission.[32] Copyright 2019, Elsevier.

Table 1. A comparison of different methods for measuring work functions.[27b,29]

Work principle	Requirements	Merits	Demerits
Photoelectric effect	• Electron spectrometer • Energy tunable photon source • Photodetector	• Compatible with UPS[a] technique • Applicable to various materials • Flexible testing conditions	• Average work functions • Ionization energy obtained for semiconductors
Thermionic emission	• High-temperature source • High-temperature resistant materials	• Relatively simple operation	• Materials need high-temperature resistance
Field emission	• Stable electron source • Materials fabricated into fine tips	• Applicable to field emission microscope (depending on crystal orientations)	• Rapid emission decay • Sensitive to tip radius and microfield • Large emission fluctuations
Contact potential difference	• Reference electrodes	• Quick measurement • High resolution • Applicable to insulators	• Results largely rely on tip conditions • Relative work function values

[a] UPS, ultraviolet photoelectron spectroscopy.

and Pt@N-0.5-CNC are calculated to be 4.74, 4.68, and 4.63 eV, respectively.

Besides photon energy, when enough thermal energy is applied to a material, some electrons with kinetic energy higher than the work function will emit and produce electric current. Governed by Richardson's law, the thermionic current is exponentially proportional to the work function. Therefore, thermionic work functions of materials can be obtained by testing the electronic current density under different temperatures.[29a] Importantly, the tested materials should be stable at high temperatures (>1000 K). In the field emission-based measurement, electrons are emitted by quantum mechanical tunneling under a high electric field. The local emission current density is described by the Fowler-Nordheim equation.[31] To enhance the field emission during the test, specimens should be made into very sharp tips. Generally, the field emission and thermionic emission-based methods are seldom used for determining the work function of electrocatalysts, due to the relatively high requirements for samples.

By testing the contact potential difference (CPD) between a reference material and the specimen, the Kelvin probe technique becomes an efficient method to measure the relative work function of materials. During the measurement, the relative surface potential can be measured by forming a capacitor between the reference material and the target material (Figure 2c).[4] The obtained CPD can be directly used to calculate the work function difference between the two materials (reference and target materials; CPD = $(\Phi_M - \Phi_R)/e$, φ_M and φ_R are the work function of the target material and reference material, respectively). Nowadays, the scanning Kelvin probe microscope reaches a nanometer-scale lateral resolution, and it can quickly measure the variation of work function during electrochemical reactions. As depicted in Figure 2d,e, the work functions of MoO_2 nanosheets (MoO_2 NSs) and Pt clusters anchored MoO_2 NSs (Pt Cs/MoO_2 NSs-L) were tested by the Kelvin probe force microscopy (KPFM), and Au film works as a standard sample to determine the work function of the tip.[32] It can be seen that the work functions of Pt Cs/MoO_2 NSs-L and MoO_2 NSs can be easily determined by recording the CPD between tip and target materials. Notably, work functions obtained by the KPFM technique are highly sensitive to the tip conditions and the measurement environment.

Besides these experimental methods, the work functions of materials can be calculated by density functional theory (DFT) methods. The electrostatic potential across the material–vacuum interface is generally calculated to determine the work function of materials.[33] Such computational methods are efficient in work function calculation and can help accelerate the design of high-performance catalysts with suitable work functions. However, the models for calculations cannot represent some real properties of materials, in terms of nanostructure, crystallinity, etc.

3. Work Function: A Catalytic Activity Descriptor

3.1. Theoretical Fundamentals of Work Function-Based Activity Descriptors

The work function of materials plays a crucial role in determining the ease of electron transfer on the surface, directly influencing the electron-donating ability or electron affinity.[34] Consequently, work function serves as a convenient metric for assessing the electron transfer rate on an electrocatalyst (electrode), essentially defining the IET at the catalyst-electrolyte interface.[35] In heterogeneous electrocatalysis, where reactions occur at the electrified interface between the solvated solid electrode and solution, the IET assumes a pivotal role and it often serves as the rate-determining step (RDS).[36] Therefore, utilizing the work function as a descriptor offers a sensible approach to predict the catalytic performance of materials.

To comprehend the fundamental principles underlying work function-based activity descriptors, it is crucial to establish a connection between the work function and the charge transfer processes. In electrocatalysis, the interaction between solid electrocatalysts and reactants (or intermediate, e.g., *OH in OER) can accelerate the reaction process. This interaction typically involves the transfer of electrons between catalysts and the adsorbed reactants, with consideration given to the Fermi level of the catalysts and the energy levels of the reactants' highest occupied molecular orbital or lowest unoccupied molecular orbital.[37] Consequently,

the catalytic behavior can be correlated with the alignment between the catalysts' Fermi level and the energy levels of the reactant orbitals, thus linking it to the catalysts' work function.[38]

The energetics of electron transfer govern the efficiency and kinetics of catalytic reactions occurring at the interface between solid catalysts and adsorbed reactants, ultimately dictating the overall performance of electrocatalytic systems. To elucidate the relationship between work function and the energetics of electron transfer, consider the interfacial electron transfer process occurring in two steps: (I) the electron is removed from the catalyst surface to a local point, incurring an energy cost equal to the local work function Φ; and then (II) the electron is transferred from the local point to reside on the adsorbate.[39] The second step results in an energy gain associated with moving the electron from the local point to the adsorbate, which should be the adsorbate electron affinity (E_A, assuming the adsorbate and electron are both in the vacuum region). In actual conditions, the adsorbate is not present in a vacuum during step (II), leading to a potential energy modification, represented by an energy gain of ΔE.[40] Therefore, the energy of an *n*-electron transfer process can be expressed as $n(\Phi - E_A - \Delta E)$.[41] When considering a series of catalysts with similar properties and assuming the E_A and ΔE terms remain relatively constant, the energy needed to transfer electrons correlates with the catalyst's work function along with a constant shift.[42] As further suggested by Lin et al., the Gibbs free energy (G_s) of binding a species (S) comprises a dominant chemical binding term proportional to the charge-transfer energy and a relatively constant charge-transfer-independent term (G_s^0), expressed as $G_s = \lambda n(\Phi - E_A - \Delta E) + G_s^0$.[38a] Here, λ represents a reaction-specific proportionality coefficient, while the E_A, ΔE, and G_s^0 terms are expected to exhibit consistency within the same catalyst family.

In electrochemical reactions, overpotentials (η, a main activity parameter) are approximated by the relative Gibbs free energies of adsorbates at the final and initial states of the RDS. This can be written as $\eta = \Delta G/ne - E^0 = (G_P - G_R)/ne - E^0$,[43] where G_R and G_P are the Gibbs free energies of the adsorbed reactant and product respectively, *n* is the electron transfer number in RDS, and E^0 is the standard reaction potential. Then, it is expected that $\Delta G = G_P - G_R = \lambda(n_P - n_R)\Phi + C$, where λ is a proportionality coefficient. The constant C represents the contributions from E_A, ΔE, and G_s^0, which remain relatively stable within a specific electrocatalyst family. Thus, an approximately linear dependence of the overpotential on the work function of catalysts is suggested.

The above analyses imply a strong correlation between the binding energies associated with electron transfer and the work function of catalysts for a given reactant. Furthermore, by correlating overpotentials in electrochemical reactions with the work function of catalysts, one can approach an approximately linear relationship between catalytic activity and the work function of catalysts. Understanding these theoretical fundamentals is crucial in predicting and optimizing the catalytic performance of materials in electrochemical systems. Of note, these correlations are not expected to be exact due to variations in factors assumed to be constant and the non-linearity of the binding energy with electron transfer. Notwithstanding, as the adsorption energies of reactants in the RDS predominantly influence the catalytic process, a correlation between the work function and catalytic activity is observed for given reactions within an electrocatalyst family.

3.2. Developments of Work Function-Based Activity Descriptors

Currently, the catalytic activity of materials for different electrochemical reactions (especially HER, ORR, CO_2RR) has been well correlated with work function. The work function-based activity descriptors have guided the understanding of catalytic mechanisms and catalyst development.

3.2.1. Hydrogen Evolution Reaction (HER)

HER is a key half-reaction in water electrolysis for sustainable hydrogen production.[44] It is suggested that the relationship between the M–H_{ad} bond strength (M: electrode materials) and the exchange current (represents HER activity) guides the design of efficient HER catalysts.[45] Materials with a suitable M–H_{ad} bond strength (not too strong nor too weak) would have the optimal activity, and Pt is considered the best metal for HER.[26b,46] Starting with Pt metal, a decrease in work function results in stronger adsorption of H on a series of *d*-metals (**Figure 3a**),[7] leading to a potential deterioration in HER performance. Dadallagei et al. conducted a survey analyzing the relationship between work function and HER activity of 31 metals, as shown in Figure 3b.[47] It can be observed that for both *d* and *sp* metals, a higher work function typically corresponds to higher HER activity, as the work function plays a role in lowering the reaction activation energy. Further considering the effect of the real HER process in water, the change in the work function of metals upon adsorption of hydrogen through the water layer is developed as a HER activity descriptor (Figure 3c). The volcano plot presents the optimal interaction of hydrogen intermediates with these metals, in the presence of water. Notably, these studies are focused on pure metals and no universal model has been reported on the work function-HER activity relationship of general materials.

Currently, there is no direct answer to this question of whether a small or a large work function benefits HER. Many studies have found that the reduced work function leads to better HER activities of catalysts (e.g., Cu_2S-Se@Cu,[9] CoFe@N-doped carbon@MoS_2,[48] Mn/Co-N-doped carbon[49]) due to the enhanced electron transfer efficiency at the electrocatalyst-electrolyte interface. In these studies, catalysts are in a complex structure and the work functions of similar materials are calculated and compared, which provide useful information for guiding the design of HER catalysts with similar properties. However, Tong and coauthors suggested that a work function closer to Pt would have better HER performance. In their study, the work functions of NF (nickel foam), Ni_3S_2/NF, Ni_3S_2-NF, and Pt/C-NF are 4.6, 4.9, 4.7, and 5.1 eV, respectively. The work function of Ni_3S_2/NF is close to that of Pt/C, contributing to its better HER performance.[50] Based on current studies, it remains highly challenging to put forward a direct relationship between work function values and HER activities of diverse catalysts, due to the huge differences in catalysts' properties (e.g., category, nanostructure, surface chemistry) and work function measurement methods.

3.2.2. Oxygen Reduction Reaction (ORR)

ORR that converts O_2 into H_2O is a key reaction in fuel cells and metal-air batteries.[51] The ORR activity of materials

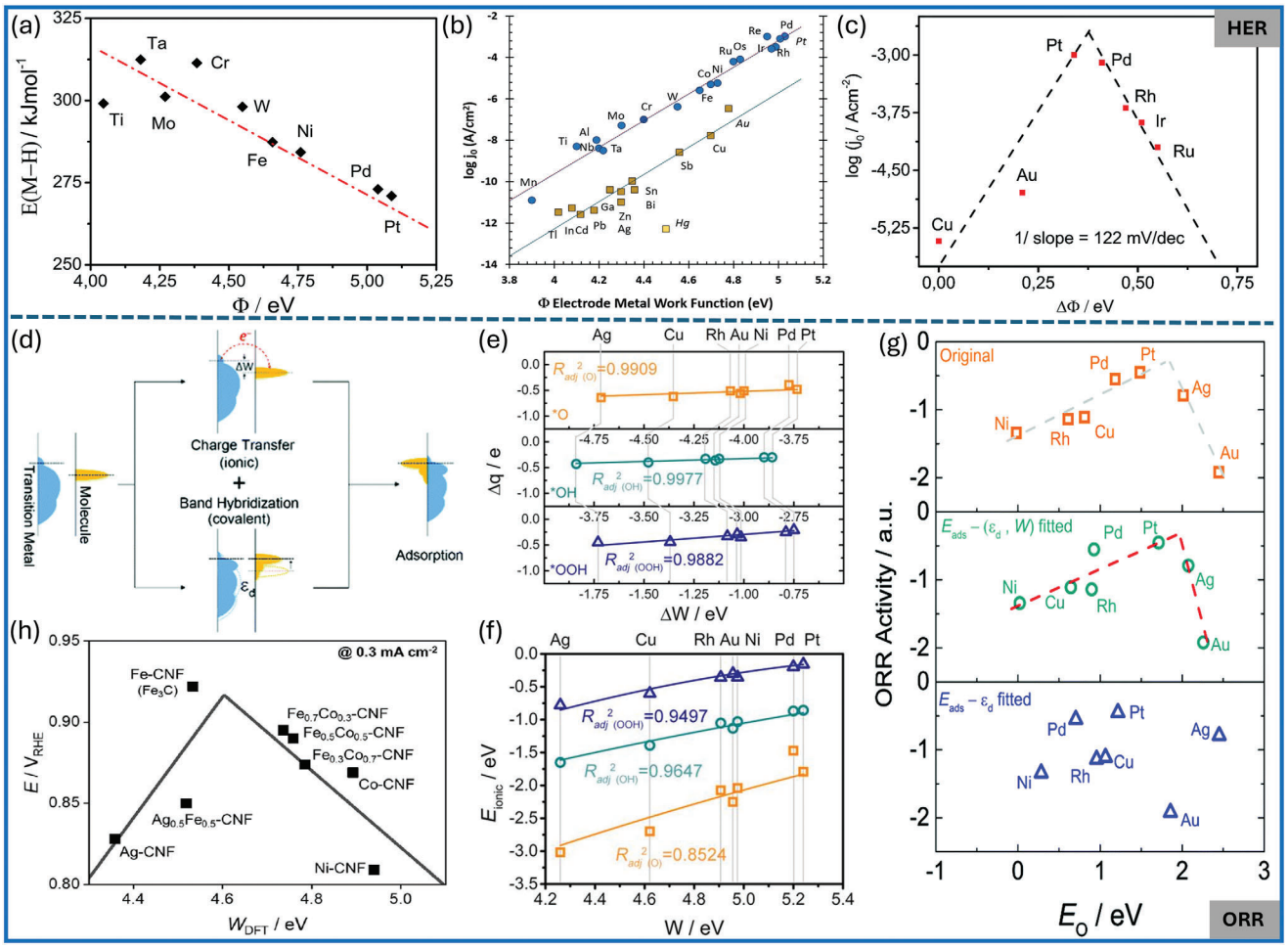

Figure 3. a) Relationship between the metal–H bond strength and work function of d-metals. Reproduced under terms of the CC-BY license.[7] Copyright 2017, The Authors, published by Royal Society of Chemistry. b) Plots of logj_0 versus work function for HER on metal electrodes. J_0: exchange current density. Reproduced under terms of the CC-BY license.[47] Copyright 2023, The Authors, published by IOP Publishing. c) Relationship between the change in the work function of metals upon adsorption of hydrogen through the water layer and the exchange current density for HER. Reproduced under terms of the CC-BY license.[7] Copyright 2017, The Authors, published by Royal Society of Chemistry. d) Illustration of the ionic and covalent bonding contributions to the adsorption of ORR intermediates on transition metals. e) Relationship between transferred charge (Δq) and the work function difference between metals and adsorbate (ΔW). f) E_{ionic} values as a function of metals' work function. g) Relationship between ORR activity of metals and (bottom) calculated E_O with the E_{ads}–ϵ_d linear fitting, (middle) calculated E_O with the E_{ads}–(ϵ_d, W) 2D polynomial fitting, and (top) DFT-simulated E_O. Reprinted with permission.[53] Copyright 2017, Royal Society of Chemistry. h) Volcano curve of the applied potential at ORR current density of 0.3 mA cm^{-2} as a function of the work function of the embedded metal. Reprinted with permission.[55] Copyright 2019, American Chemical Society.

is mainly determined by the adsorption energy (E_{ads}) of reactants/intermediates, especially *OH, *O, and *OOH.[52] Shen et al. divided the E_{ads} of ORR intermediates into two parts, including ionic (E_{ionic}) and covalent ($E_{covalent}$) contributions (Figure 3d).[53] The E_{ionic} part determined by the charge transfer between the adsorbed reactants/intermediates and materials (Δq) can be related to the work function, while the $E_{covalent}$ is determined by the *d*-band center (ϵ_d). Thus, the E_{ads} of reactants/intermediates can be obtained via the work function and *d*-band properties of metals. As displayed in Figure 3e, Δq values for *OOH, *OH, and *O adsorption exhibit a strong relationship with the work function difference between metals and adsorbates (ΔW). A larger ΔW value leads to a smaller Δq. Further analysis suggests that the E_{ionic} is in proportion with the work function of metals, and Pt with the largest work function possesses the smallest E_{ionic} (Figure 3f). Compared with conventional ϵ_d-determined E_{ads}, the E_{ads}–(ϵ_d, *W*) 2D polynomial correlation exhibits an upgraded accuracy. Especially, the volcano relationship between the oxygen binding energy (E_O) of metals and the ORR activity shows a significantly improved accuracy when the 2D polynomial fitting function is applied for E_O calculation (Figure 3g). This study integrates the work function and *d*-band center for the accurate determination of intermediate adsorption energy, which helps understand the role of the work function in ORR activity analysis.

The direct relationship between work function and ORR activity/selectivity of catalysts has been investigated. For carbon-based electrocatalysts (such as graphene and doped-porous carbon), it has been found that a smaller work function can

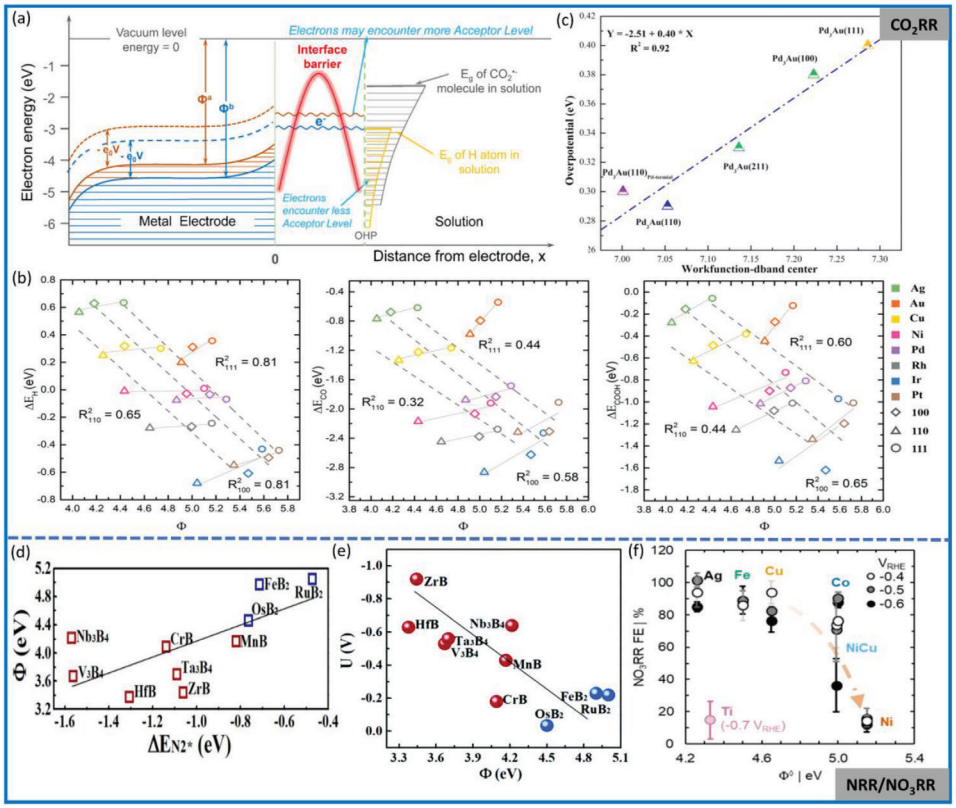

Figure 4. a) Scheme of the influence of work function and applied external potential on the electron transition probability, electronic state density in metal, and existence probability, in the CO_2RR process. Reprinted with permission.[36] Copyright 2019, American Chemical Society. b) Relationship of working functions versus intermediate adsorption energies on metals with different facets. (left) H, (middle) CO, and (right) COOH. Reprinted with permission.[57] Copyright 2020, American Chemical Society. c) Relationship between the overpotential of the diverse surfaces of Pd_3Au and the difference between work function and d-band centre. Reprinted with permission.[58] Copyright 2023, Royal Society of Chemistry. d) Relationship between work function and N_2 adsorption energy for MBenes. e) NRR onset potential versus work function of Mbenes. Reprinted with permission.[60] Copyright 2020, Royal Society of Chemistry. f) NO_3RR Faradaic efficiency versus work function of metals. Reprinted with permission.[61] Copyright 2022, American Chemical Society.

contribute to a better ORR activity and a higher electron transfer number (approaching four).[4,54] In these studies, it is proposed that the energy needed for the oxygen reduction reaction (ORR) can be decreased by reducing the work function through the creation of additional electroactive sites. According to Oh et al., introducing heteroatoms and increasing the number of edge sites on graphene-based catalysts can lower the work function, resulting in a reduced energy barrier. This facilitates the transfer of electrons from the catalyst surface to adsorbed oxygen molecules, ultimately enhancing the ORR activity.[54b] However, when investigating the ORR activity of a series of metal-embedded carbon core–shell materials, a volcano curve of the ORR activity as a function of the work function of the embedded metals is suggested (Figure 3h).[55] DFT calculations verify that the surface area normalized number of electrons transferred from metals to carbon (ΔQ_{ET}) shows a linear relationship with the variation in the work function of metal catalysts. Additionally, the ΔQ_{ET} is correlated with the ΔE_O of composite materials. Therefore, the work function of embedded metals can affect the ORR activity by tuning the oxophilicity and electronic properties of the outer carbon layer.

3.2.3. Carbon Dioxide Reduction Reaction (CO_2RR)

Electrochemically converting CO_2 into fuels and chemicals is an important method for carbon utilization and reducing global carbon emissions. In the CO_2RR process, the generation of the first reaction intermediate ($CO_2^{\bullet-}$) has been considered as a thermodynamic and kinetic bottleneck.[56] In the $CO_2(g) + e \rightarrow CO_2^{\bullet-}$ process, the IET at the catalyst–solution interface is a rate-determining step. Under the same applied potential, a material with a lower work function possesses a higher IET efficiency. Of note, the effect of work function on the catalyst–solution IET is largely determined by the extent of overlap between equal energy levels of electrons in solvated CO_2 and the material (**Figure 4a**).[36] Thus, decreasing the work function of materials (e.g., Ag electrode) can cause the Fermi level to shift upward and trigger more electrons to transfer to CO_2 acceptor levels, as well as lowering the energy barrier height. Limiting HER is important for enhancing CO_2RR selectivity. For the Ag electrode with a smaller work function, the acceptor levels of CO_2 are much more than those of H^+ in the electrolyte, and the probability of electron transfer from the electrode to CO_2 is higher than that to H^+. Accordingly,

the CO_2RR selectivity can be increased by decreasing the work function of the Ag electrode.

Besides considering the formation of $CO_2^{\bullet-}$, the adsorption strength of reaction intermediates like H*, CO*, and COOH* are critical for CO_2RR catalyst design. As shown in Figure 4b, the work functions of metals show a roughly linear correlation with the adsorption energies of these reaction intermediates.[57] Also, the facet of metals affects the work function, as well as the adsorption energy of intermediates. Zheng et al. further found a linear relationship between the CO_2RR (CO_2-to-formic acid) overpotential and the difference in the work function and *d*-band center of Pd_3Au catalyst's different surfaces (Figure 4c).[58] The (111) facet of Pd_3Au with the highest work function (≈7.3 eV) exhibits the worst catalytic performance.

3.2.4. Nitrogen/Nitrate Reduction Reaction (NRR/NO_3RR)

The electrochemical reduction of N_2 and NO_3^- is a promising route to produce NH_3 which is an important chemical for various industries.[59] For NRR over a series of MBene catalysts, a correlation between the N_2 adsorption energies and work functions has been suggested (Figure 4d,e).[60] Generally, MBenes with a larger work function exhibit a weaker N_2 binding strength and a lower onset potential. Catalysts FeB_2, RuB_2, and OsB_2 with boron active surfaces exhibit higher work functions compared to their counterparts with metal active surfaces. This characteristic contributes to a more suitable adsorption capacity towards N_2. Therefore, FeB_2, RuB_2, and OsB_2 show higher NRR activity. In Figure 4d,e, some data points deviate from the linear relation, implying that there should be other factors that affect the NRR property of MBenes.

For NO_3RR, the work function has been used to correlate with the reaction Faradaic efficiency (FE) which represents the electron selectivity between NO_3RR and HER (Figure 4f).[61] The NO_3RR FE is high (over 70%) for metals with relatively low work functions (<5 eV) and relatively low H chemisorption energies (e.g., Fe, Co, Ag, and Cu), while it reduces for metals with either a high work function (Ni) or a high H chemisorption energy (Ti). With a high work function, Ni shows a low NO_3RR FE due to the facile H–H coupling kinetics. This is because high work functions could provide nominally negatively charged surfaces that can attract protons electrostatically. Although Ti has a low work function, the strong H chemisorption strength will form an H*-saturated surface that limits nitrate adsorption.

3.2.5. Electro-Oxidation Reactions

Electrochemical oxidation reactions like OER, hydrogen oxidation reaction (HOR), UOR, and glycerol oxidation reaction (GOR) are key reactions in green energy systems. Different from electrochemical reduction reactions, the relationship between catalysts' work function and their catalytic performance is less explored. Several studies have investigated the work function-catalytic activity relationship of perovskite oxides, such as $La_{0.9}Fe_{0.92}Ru_{0.08}O_{3-\delta}$ (**Figure 5a**),[62] $Ba_xLa_{2-x}CoMnO_{6-\delta}$ (Figure 5b),[63] and $Sr_{0.9}Ce_{0.05}Fe_{0.95}Ru_{0.05}O_3$ (Figure 5c).[64] In these perovskite systems, a smaller work function is correlated with a higher OER activity. A low charge-transfer barrier can be attained with a small work function, which further accelerates the charge-transfer process and ultimately facilitates the OER process. For OER/ORR bifunctional catalysts, the potential gap ($\Delta E = E_{OER} - E_{ORR}$) is generally used to describe the ORR/OER bifunctional activity. For a series of Fe/Co/Ni-modified MXene-based double-atom catalysts (DACs) (Figure 5d),[65] it is found that the work function of the DACs can reveal the essence of the bifunctional catalytic activities. When the work function of the catalyst approaches 5.67 eV, the ΔE value decreases, leading to higher bifunctional catalytic activity (Figure 5e). For GOR over transition metals, Sivasakthi et al. have suggested a linear correlation of the work function of metals with the experimental peak current density (Figure 5f), and a higher work function leads to a better GOR activity.[66] In these studies, how the work function determines the atomic-level catalytic processes remains unclear.

Current studies on the work function-based activity descriptors indicate that work function is a promising and important indicator of materials' catalytic activities, while the development of work function-based descriptors is still in the early stages and is involved in limited reactions. For most involved electrochemical reactions, the investigated catalysts only cover several types of catalysts (e.g., metals, MXenes, alloys), and a general work function-based descriptor for diverse electrocatalysts is still unavailable.

4. Work Function-Regulated Material-Electrolyte IET for Monolithic Catalyst Design

Guided by the work function-based activity descriptors, the material-electrolyte IET plays a vital role in determining the catalytic performance. By manipulating the physicochemical properties, one can control the work function of monolithic electrocatalysts, thus upgrading the catalytic performance (**Table 2**). Considering the work function regulated material–electrolyte IET, the design philosophy focuses on the correlation between regulated work function value and catalytic performance. Monolithic catalysts mentioned in this section refer to those catalysts designed with the work function-regulated material–electrolyte IET, no matter the phase composition (monophase or multiphase).

4.1. Carbon Catalysts

Earth-abundant carbon materials with redox activity (e.g., graphene, carbon nanotubes (CNTs), porous carbon) are favorable alternatives to the noble metals-based electrocatalysts, especially for ORR and HER applications. By engineering the work function of carbon materials, it is feasible to optimize the catalytic activity of carbon catalysts. Generally, heteroatom doping and defect engineering are employed to regulate the work function of carbon materials.

4.1.1. N Doping

Nitrogen-doped carbon is the most sophisticated carbon-based electrocatalyst, which can be directly obtained from carbon and nitrogen precursors via one-step pyrolysis.[84] The species and

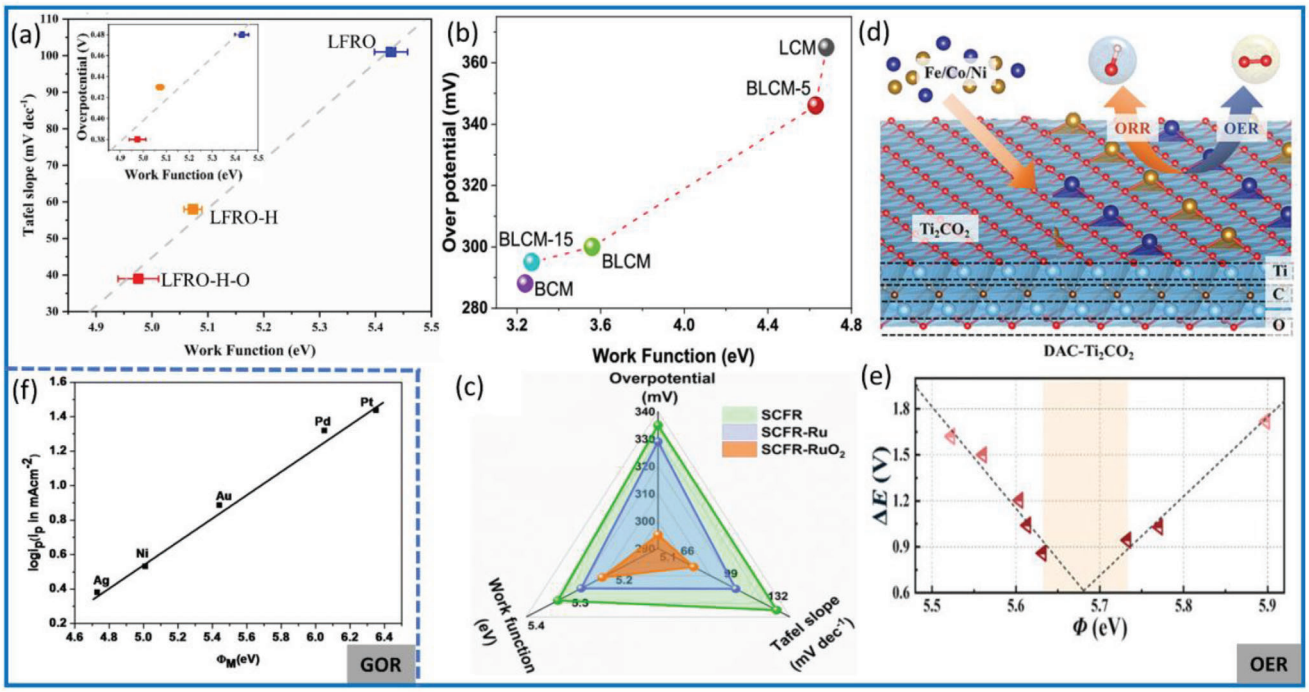

Figure 5. a) Correlation between OER activities (Tafel slopes, overpotentials) and work functions for LFRO ($La_{0.9}Fe_{0.92}Ru_{0.08}O_{3-\delta}$), LFRO-H (LFRO reduced in 5% H_2/N_2), and LFRO-H-O (LFRO-H oxidized in air). Reprinted with permission.[62] Copyright 2021, Elsevier. b) Relationship between work function and OER overpotential over BCM (2H-$Ba_2CoMnO_{6-\delta}$), LCM ($La_2CoMnO_{6-\delta}$), and BLCM ($Ba_xLa_{2-x}CoMnO_{6-\delta}$). Reproduced under terms of the CC-BY license.[63] Copyright 2022, The Authors, published by American Chemical Society. c) Relationship between OER activities (Tafel slopes, overpotentials) and work function of the SCFR ($Sr_{0.9}Ce_{0.05}Fe_{0.95}Ru_{0.05}O_3$), SCFR-Ru, and SCFR-$RuO_2$. Reprinted with permission.[64] Copyright 2023, Royal Society of Chemistry. d) Fe/Co/Ni-diatomic catalysts (DAC) on Ti_2CO_2 and for the OER/ORR application. e) Correlation between bifunctional potential difference (ΔE) and work function for catalysts. Reprinted with permission.[65] Copyright 2021, Wiley-VCH. f) Relationship between the logarithm of peak current density for glycerol oxidation and work function of metals. Reprinted with permission.[66] Copyright 2019, Royal Society of Chemistry.

contents of nitrogen dopants are highly related to the work function of N-doped carbon.[85] As depicted in **Figure 6a**, graphitic N, pyrrolic N, pyridinic N, and oxidic N are universally found in N-doped carbon,[86] and the formation of different nitrogen species is sensitive to nitrogen precursors and pyrolysis temperature.[87] A general trend is that N dopants can reduce the work function of carbon materials. In pure pyridinic N-doped graphene, the introduction of 16% pyridinic N (N/C atomic ratio) can reduce the work function by 0.2 eV. For the ORR application, the pyridinic N dopant in the graphene catalyst benefits the 2e pathway.[88] The work function-dependent ORR pathway/selectivity over heteroatom-doped carbon is also suggested by Cheon et al., who found that a lower work function led to a higher electron transfer number (Figure 6b).[8] Compared with dual-doped, mono-doped, and undoped ordered mesoporous carbon (OMC), the N, S, and O tri-doped OMC with the lowest work function (<4.8 eV) exhibits the highest electron-transfer number of about 3.5. In addition, the ORR kinetic activity of carbon materials is inversely proportional to their work function, and N, S, and O tri-doped OMC outperforms its counterparts (Figure 6c). This study implies that introducing more dopant species holds the promise to regulate the work function of carbon materials to a large degree.

Specific types of carbon defects can be formed through controllable nitrogen doping, and these carbon defects are generally active sites for electrochemical reactions. Regulating the work function of local carbon structure by introducing N dopant and defects has been used to develop high-performance ORR catalysts. By controlling the pyrolysis temperature, Bhardwaj et al. developed a series of defective N-doped carbon. The sample obtained at 1050 °C ($DG_{1:1}$-1050, 1:1 means the ratio of melamine and zinc in precursors) has a high defect level and a high ratio of pyridinic and pyrrolic nitrogen dopants (Figure 6d).[67] The co-manipulation of N dopants and defects in DG-1050 leads to a lower work function of 3.72 eV than the counterparts, ultimately contributing to a higher ORR activity (Figure 6e,f). Considering the relationship between work function and ORR activity, it is sensible to identify the active sites (e.g., defects, dopants) on carbon materials by testing the local work function of a specific area. For example, in a highly oriented pyrolytic graphite with specific pentagon defect sites (D-HOPG), the local work function shows a positive correlation with the count of the exposed edges (**Figure 7a-c**).[89] With more edge sites, the pentagon defect (Site 2) has a lower work function. In return, the pentagon defects at the edge surface exhibit higher ORR activity than those sites in the top or bottom regions of carbon (Figure 7d).

4.1.2. N-Free Heteroatom Doping

Besides nitrogen doping, introducing other heteroatoms into carbon materials also can regulate the work function.

Table 2. A Summary of work function (Φ)-guided design of monolithic catalysts.

Catalyst	Method for φ regulation	Catalytic reaction	Catalytic performance
S-doped carbon[54c]	S doping	ORR	E_0[a]: 0.84 V vs RHE[b]
N, S, and O co-doped porous carbon[8]	N, S, and O co-doping	ORR	E_0: 0.85 V vs RHE
N-doped defective carbon[67]	N doping, defect construction	ORR	$E_{1/2}$[c]: 0.82 V vs RHE
N-coordinated Co, Mn co-doped carbon[49]	Co, Mn co-doping	HER	η_{10}[d]: 116 mV, Tafel slope: 58 mV dec^{-1}
GO-Fe-N[e][4]	Fe, N co-doping	ORR	E_0: 1.05 V vs RHE, $E_{1/2}$: 0.87 V vs RHE
N-Doped Mo_2C[68]	N doping	HER	η_{10}: 39 mV, Tafel slope: 69 mV dec^{-1}
$CoSe_{1.28}S_{0.72}$[2a]	S doping	HER	η_{10}: 67 mV, Tafel slope: 50 mV dec^{-1}
$Co_{1.75}Al_{1.25}O_4$[69]	Al doping	OER	η_{10}: 248 mV, Tafel slope: 80.6 mV dec^{-1}
Fe-doped $W_{18}O_{49}$[70]	Fe doping, vacancy engineering	NRR	NH_3 yield: 24.7 μg h^{-1} mg_{cat}^{-1}, FE: 20% (−0.15 V vs RHE)
PdBi[10]	Strain engineering	ORR	SA[f]: 2.07 mA cm^{-2} (0.85 V vs RHE)
$Ba_5Co_{4.17}Fe_{0.83}O_{14-\delta}$[71]	Strain engineering	OER	η_{10}: 335 mV
PdIr bimetallene[72]	Strain engineering	FAOR[g]	MA[h]: 2.70 A mg_{Pd+Ir}^{-1} (0.5 V vs RHE)
Cu_2S-Se@Cu[9]	Vacancy engineering	HER	η_{100}: 315 mV, Tafel slope: 97 mV dec^{-1}
Defective VS_2[73]	Vacancy engineering	NRR	NH_3 yield: 20.29 μg h^{-1} mg_{cat}^{-1}, FE: 3.86% (−0.6 V vs RHE)
Ag powder[74]	Facet engineering	CO_2RR	FE of CO: 91%
$In_{0.17}Ru_{0.83}O_2$[75]	Component regulation	OER	η_{10}: 177 mV, Tafel slope: 32.62 mV dec^{-1}
$Au_{20}Ag_{80}$[11]	Component regulation	CO_2RR	FE of CO: 68 7%
Pt_3V[76]	Component regulation (alloying)	HER	η_{10}: 20 mV, Tafel slope: 36 mV dec^{-1}
TePbPt alloy nanotube[77]	Component regulation (alloying)	MOR[i]	MA: 532.35 mA mg_{Pt}^{-1} (0.6 V vs RHE)
Nanostructured Au[12]	Nanostructure control	CO_2RR	FE of CO: > 90%
WSe_2 flakes[78]	Nanostructure control	CO_2RR	FE of CO: 24%
MoS_2 quantum dots[79]	Nanostructure control	NRR	NH_3 yield: 39.6 μg h^{-1} mg_{cat}^{-1}, FE: 12.9% (−0.3 V vs RHE)
defective carbon-CoP[80]	Composite construction	OER	η_{10}: 320 mV, Tafel slope: 52.5 mV dec^{-1}
$FeSe_2$-$MoSe_2$/rGO[81]	Composite construction	HER	η_{10}: 101 mV, Tafel slope: 55 mV dec^{-1}
Fe SAs/NC[j][82]	SAC construction	ORR	$E_{1/2}$: 0.84 V vs RHE
NiMn DAC[83]	DAC construction	CO_2RR	FE of CO: 98.3%

[a] E_0, onset potential; [b] RHE, reversible hydrogen electrode; [c] $E_{1/2}$, half-wave potential; [d] η_{10}, overpotential at the current density of 10 mA cm^{-2}; [e] GO-Fe-N, Fe and N co-doped graphene oxide; [f] SA, specific activity; [g] FAOR, formic acid oxidation reaction; [h] MA, mass activity; [i] MOR, methanol oxidation reaction; [j] Fe SAs/NC, Fe single atoms on N-doped carbon.

Nonmetallic dopants like boron,[54a] phosphorus,[90] and sulfur[54c] are used to reduce the work function of carbon. Although these dopants can help decrease the work function, there is no strict correlation between doping level and work function. In a series of B-doped onion-like carbon (B-OLC) prepared with various boric acid amounts (5, 10, and 20 wt%), the contents of B in the resulting B-OLC-1-5, B-OLC-1-10, and B-OLC-1-20 are 1.15 at%, 2.24 at%, and 3.98 at%, respectively (Figure 7e).[54a] B-OLC-1-10 with a medium level of B dopant possesses the smallest work function (Figure 7f), as well as the highest conductivity. These features contribute to a higher ORR activity. Moreover, a linear relationship between the work function and ORR electron transfer number is found, and a higher electron transfer number is accompanied by a lower work function, in line with the heteroatom-doped ordered mesoporous carbon reported by Cheon et al.[8] Multiple doping further benefits the flexible modification of work function. In a Ge and P co-doped carbon, the Ge/P co-doping configurations affect the computed work function. The work functions gradually increase by decreasing the number of P atoms coordinated to the Ge dopant, which are 4.23 eV (GeP_4 + PC_3), 4.27 eV (GeP_3C), 4.39 eV (GeP_2C_2), and 4.77 eV ($GePC_3$).[91] For engineering a N-coordinated graphitic carbon material (NGC) for HER, the co-introduction of Mn and Co dopants can reduce the work function of NGC to 3.5 eV, which is more beneficial for HER than the mono-doped Co-NGC (4.0 eV) and Mn-NGC (3.7 eV).[49]

With high cost-effectiveness, carbon materials are attractive electrocatalysts for diverse catalytic reactions, especially reduction processes. Through heteroatom doping, the work function of carbon materials can be easily adjusted. For the predominant nitrogen doping, it is necessary to identify and regulate the contents of specific nitrogen species, which can help to optimize the work function value. In addition, multi-heteroatom doping is capable of regulating the work function of carbon more flexibly due to the potential synergistic effect of different dopants. Carefully clarifying the relationship between doping level and work function

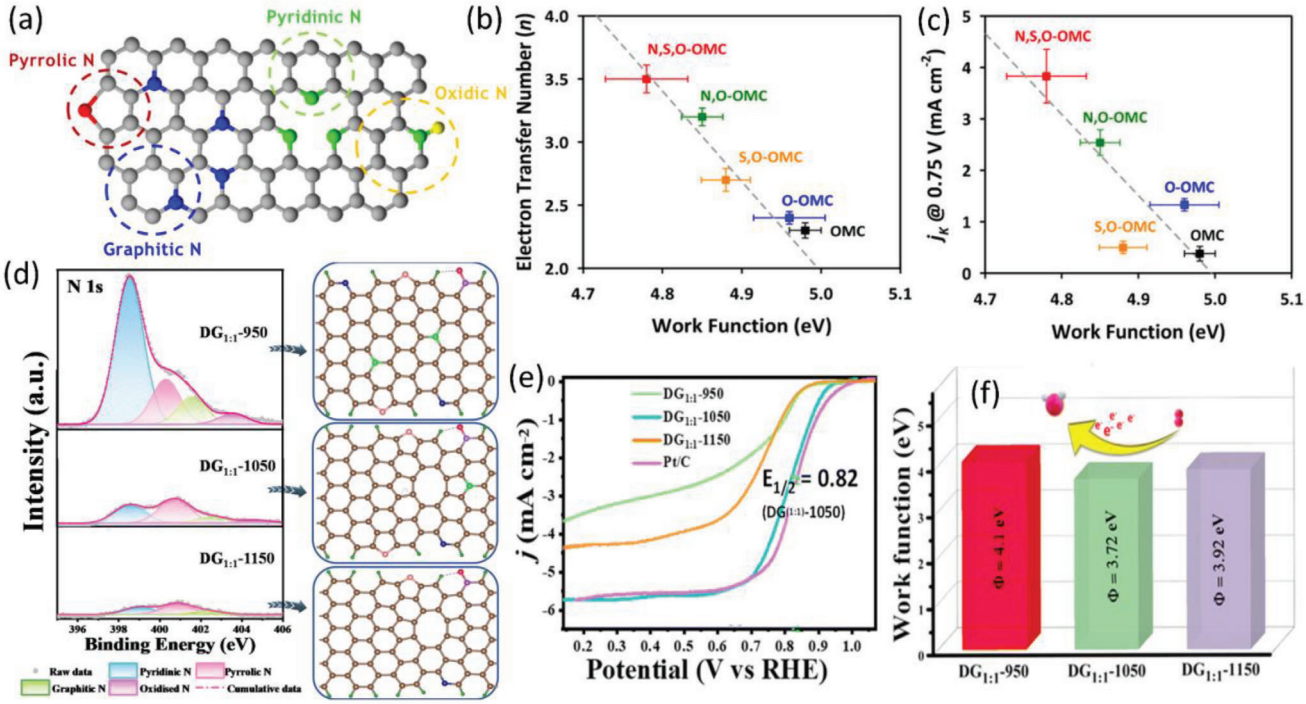

Figure 6. a) Scheme of nitrogen dopant species in a representative carbon structure. Reprinted with permission.[86] Copyright 2019, Elsevier. Correlation of ORR b) selectivity and c) activity of the doped OMCs with their work functions. Reprinted with permission.[8] Copyright 2014, American Chemical Society. d) XPS N 1s spectra and corresponding structure models in $DG_{1:1}$-950, 1050, and 1150. e) ORR polarization curves of $DG_{1:1}$-950, 1050, and 1150, as well as the Pt/C catalyst. f) Work functions of $DG_{1:1}$-950, 1050, and 1150. Reprinted with permission.[67] Copyright 2023, Royal Society of Chemistry.

is important, which can avoid misleading conclusions obtained with one or two doping levels. It should be noted that the doping process usually creates defects in carbon materials,[92] and how the dopant and defect co-regulate the work function deserves further exploration.

4.2. Metal-Based Catalysts

With flexible electronic properties, metal-based catalysts attract great interest in diverse electrocatalytic reactions. Designing efficient metal catalysts by tuning the work function has been well demonstrated, and effective strategies like defect engineering, nanostructure control, heteroatom doping, chemical component regulation, and single-atom catalyst construction are illustrated here.

4.2.1. Defect/Vacancy Engineering

The introduction of defects/vacancies into catalyst crystal structures can lead to prominent variations in electronic properties.[93] Generally, defects/vacancies can reduce the work function of catalysts and contribute to enhanced catalytic performance.[94] For example, the S defect in SnS_{2-x} can reduce the work function from 6.318 to 5.473 eV (**Figure 8a**),[95] and thus SnS_{2-x} has a stronger ability for the back-donation of electrons to the absorbed NO reactant (Figure 8b), which promotes the NO activation and further protonation steps. Assisted by molecular dynamics (MD) simulations, it can be found that SnS_{2-x} has a higher NO coverage compared to SnS_2, and SnS_{2-x} shows a stronger interaction with NO than SnS_2 (Figure 8c,d). Additionally, the Sn-V_S site in SnS_{2-x} can preferentially absorb *NO over *H (Figure 8e), suggesting that the introduction of S defects aids in inhibiting HER and improving the selectivity for NO reduction reaction (NORR). As a result, SnS_{2-x} delivers a higher NH_3 yield rate (78.6 μmol h^{-1} cm^{-2}) and a higher NH_3-FE (90.3%) than SnS_2 (Figure 8f). Similar positive effects of anion vacancies in VS_2,[73] $SmMn_2O_5$,[96] and Cu_2S-Se[9] in increasing catalytic performance by decreasing the work functions of catalysts have been verified.

However, not all the defect-induced reduced work functions can benefit the catalytic activity. In a series of OER/ORR bifunctional $Pb_2Ru_2O_{7-x}$ catalysts with various oxygen vacancy levels, a clear relationship is observed between the enhancement in ORR-specific activity and the decrease in work function. Differently, the OER activity does not follow a similar monotonous trend. At the same temperature, the air-annealed oxides have better OER activities than the Ar-annealed counterparts, which is ascribed to the lower work function of the latter. In this situation, the work function should be a semiempirical descriptor for OER over the $Pb_2Ru_2O_{7-x}$ catalysts because it could not capture the whole catalytic process including electron transfer efficiency, hydroxide affinity, and intermediate binding strength, wherein the formation of ·OOH and ·O species is the potential determining step.[97] In this context, the defect/vacancy level should be thoroughly investigated when one focuses on the relationship between defects,

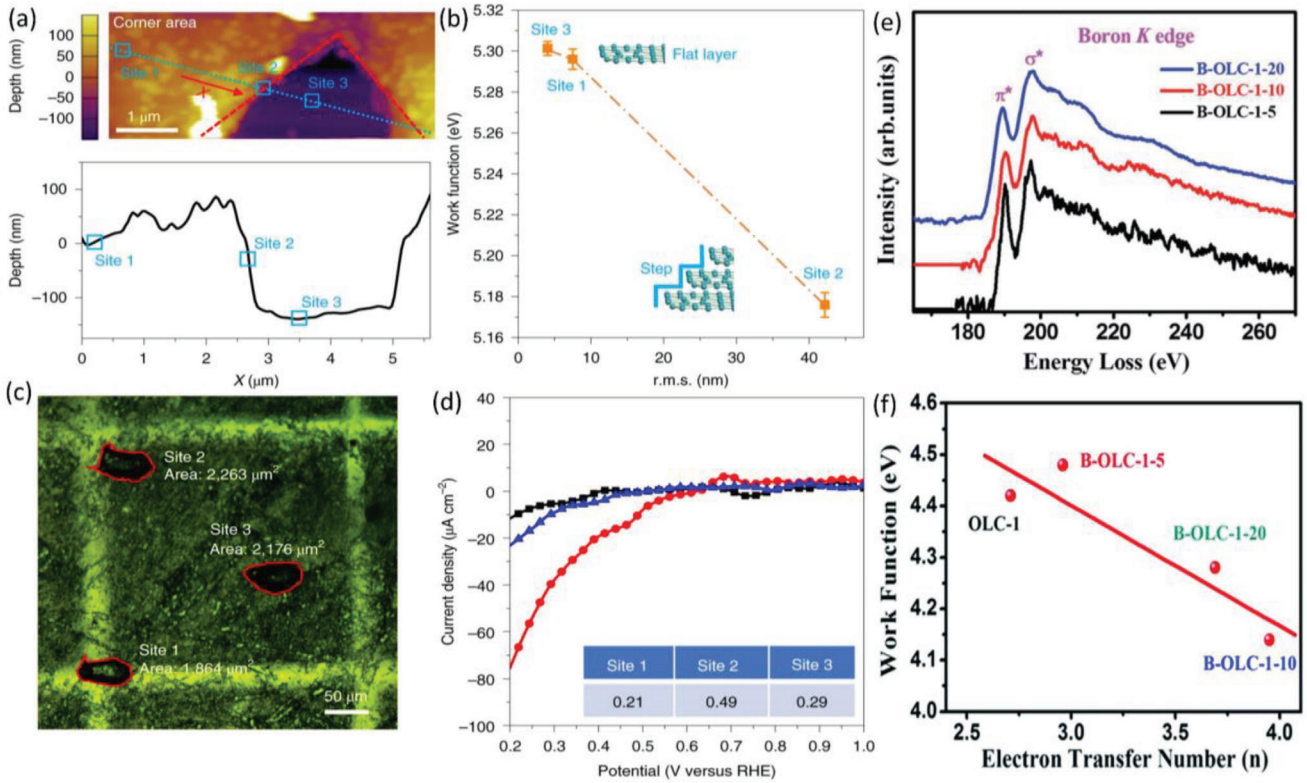

Figure 7. a) Atomic force microscopy line scan of the depth in D-HOPG. b) Correlation of the roughness and local work function values obtained at different areas on D-HOPG. c) Optical microscope image of D-HOPG. Red lines represent electrolyte droplets. d) ORR polarization curves of Site 1 (black curve), 2 (red curve), and 3 (blue curve) on D-HOPG. Inset shows the onset potentials of different sites. Reprinted with permission.[89] Copyright 2019, Springer Nature. e) Electron energy loss spectroscopy profiles of B-OLC catalysts. f) Relationship between work function and electron transfer number during ORR for different catalysts. Reproduced under terms of the CC-BY license.[54a] Copyright 2015, The Authors, published by Royal Society of Chemistry.

work function, and catalytic performance for typical catalytic reactions.

4.2.2. Lattice Strain

Lattice strain caused by bond length variations or lattice dislocation/misalignment can raise electrocatalytic activity by decreasing the work function of catalysts.[98] In most cases, a higher strain level leads to a lower work function, which contributes to enhanced catalytic performance. This trend has been verified in the $NiS_{0.5}Se_{0.5}$ (for OER),[99] Pd_8Ir_2 (for HER),[72] and $Ba_5Co_{4.17}Fe_{0.83}O_{14-\delta}$ (for OER)[71] systems. However, the study by Sarker et al. shows some different features.[10] They have developed a series of Pd-Bi catalysts with various strain levels (up to 9%) for ORR. Under the strain of up to 3%, the monotonic decrease of work function contributes to gradually increased oxygen adsorption energy ($E_{ads}O^*$), implying better ORR activities. Increasing the strain level to 5%, the work function shows an unexpected increase and thus a reduced ORR activity. Over the strain level of 5%, the ORR activity again starts increasing in strain levels of 7% and 9%, correlating with the decreased work function and improved $E_{ads}O^*$. This study emphasizes the critical role of strain level in regulating the work function and catalytic performance of metal catalysts. As such, it is necessary to analyze the relationship between work function, strain level, and catalytic performance for optimizing the catalyst design process.

4.2.3. Facet Engineering

The crystal facet of crystalline catalysts can predominately determine the catalytic performance. This is because different facets show variations in surface electronic properties (e.g., surface energy, coordination number (CN), work function).[100] In this context, controlling the exposure of crystal facets is capable of regulating the work function of catalysts. For example, Ma et al. found that the surface work functions of (111), (110), and (100)-Cu_2O were 5.00, 4.95, and 4.92 eV, respectively.[101] To optimize the catalytic performance of Ag catalysts, Luo and co-authors have reported a ball milling strategy to control the exposed crystal facets. With the milling time increased from 2 to 6 h, the ratio of Ag(110) to Ag(100) is improved (Figure 8g).[74] Furthermore, a higher Ag(110)/Ag(100) ratio contributes to a lower work function and a smaller CN (Figure 8h). The correlation between work function and CN is also applicable to Cu and Au materials, exhibiting its good universality. Further CO_2RR tests indicate that

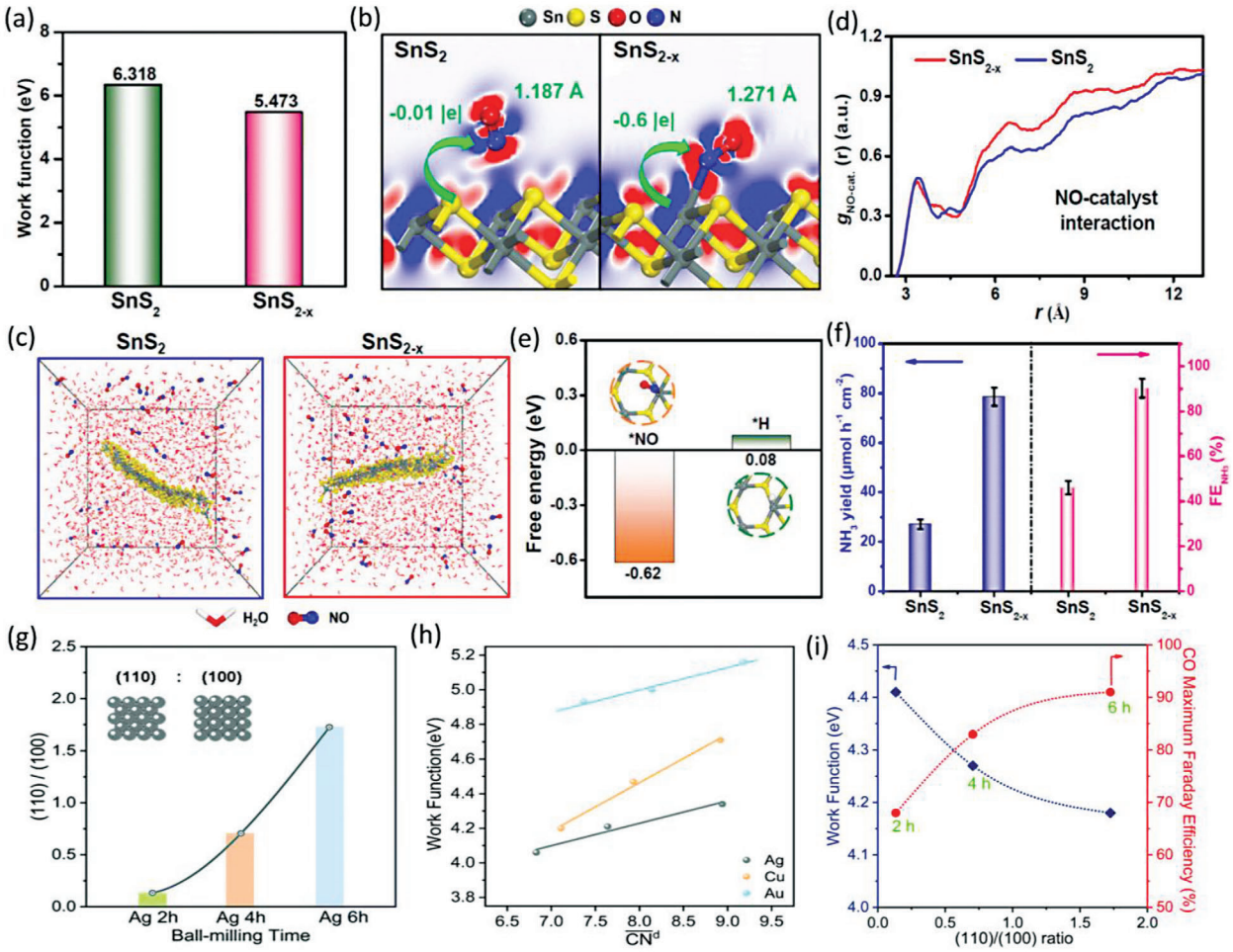

Figure 8. a) Work functions of SnS_2 and SnS_{2-x}. b) Electron contour profiles of NO adsorption on SnS_{2-x} and SnS_2 (Red color means charge accumulation and Blue color represents charge depletion). c) Snapshots of the final state of NO adsorption on SnS_2 and SnS_{2-x} after MD simulations, and the related d) radial distribution function curves. e) Free energies of *H and *NO adsorption on SnS_{2-x}. f) NORR activities of SnS_{2-x}/CC and SnS_2/CC. Reprinted with permission.[95] Copyright 2023, Royal Society of Chemistry. g) Crystal plane intensity of Ag powders milled for different periods. h) Relationship between work function and coordination number for different facets of Ag, Au, and Cu. i) Relationship of Ag(110)/Ag(100) with work function and CO faradaic efficiency for Ag catalysts. Reprinted with permission.[74] Copyright 2022, Royal Society of Chemistry.

the Ag(110)/Ag(100) ratio is negatively correlated with work function, while positively with the CO faradaic efficiency (Figure 8i). This work not only unveils the relationship between the crystal facet and the work function of materials but also provides a powerful method to shape the exposure of favorable facets of catalysts via ball milling.

4.2.4. Heteroatom Doping

Heteroatom doping is a universal technique to regulate the electronic properties of electrocatalysts.[102] Currently, many studies have incorporated dopants to tune the work function of metal catalysts, thereby contributing to regulated catalytic performance.[14,68–69,75,103] Both anion (such as N[68]) and cation (e.g., Al,[104] V,[14,103a] In,[75] Pd,[103b] Cr,[105] and Co[106]) dopants have been investigated for altering the work function of diverse metal catalysts. In most of these examples, only one dopant level is investigated, and the introduction of dopants leads to a reduced work function and ultimately a better catalytic performance. For instance, the introduction of In into the RuO_2 catalyst reduces the work function from 4.85 to 4.68 eV. The lower work function of $In_{0.17}Ru_{0.83}O_2$ benefits the electron transfer process between the reactant and the catalyst and contributes to an enhanced OER performance in the acidic electrolyte.[75] However, not all doping processes lead to a decrease in work function. Zhang et al. found that S substitution on the surface of MoC could increase the work function from 5.47 to 5.51 eV. Still, the S treatment leads to an upshifted valence band towards the Fermi level by 1.37 eV and increases the chemisorption ability towards H during HER.[107] Therefore, the effect of doping on the work function and the resulting catalytic performance of metal catalysts for different reactions should be carefully checked on a case-by-case basis.

For a thorough comprehension of the impact of dopants on work function and to tailor the work function of doped metal

catalysts for specific catalytic reactions, it is essential to study the work function dependence on the doping level.[106] Several studies uncover that the work function has an inverted volcanic-type curve relationship with the doping level and a negative correlation with catalytic activity.[14,69,106] In a V-doped MoS_2 catalyst, a moderate doping level of 5% yields the lowest work function of 5.29 eV, thereby enhancing the HER performance optimally.[14] Similarly, in a series of Al-doped Co_3O_4 catalysts, $Co_{1.75}Al_{1.25}O_4$ outperforms its counterparts ($Co_{1.5}Al_{1.5}O_4$, $Co_{2.1}Al_{0.9}O_4$, $Co_{2.4}Al_{0.6}O_4$, and Co_3O_4) for OER due to its smallest work function.[69] In-depth analysis indicates that the high performance of $Co_{1.75}Al_{1.25}O_4$ is also associated with its highest relative amount of electrophilic O_2^{2-}/O^- species (44%) and the lowest Co^{2+}/Co^{3+} ratio (0.825). These examples strongly indicate the significance of determining the optimal doping level to achieve an appropriate work function for metal catalysts.

4.2.5. Chemical Composition Optimization

Given that different elements possess distinct work functions, it is logical to fine-tune the work function of metal catalysts by optimizing the chemical composition. Partially replacing metal sites in metal-organic frameworks (MOFs) with foreign elements can alter the work function which can be further optimized by finely tuning the ratio of metals. To augment the OER/ORR efficiency of the Zn-based zeolite imidazole framework (ZIF), Co is introduced. $Zn_{0.8}Co_{0.2}$ ZIF has a smaller work function of 3.623 eV than the bare Zn ZIF (3.718 eV) and $Zn_{0.6}Co_{0.4}$ ZIF (3.659 eV). Therefore, $Zn_{0.8}Co_{0.2}$ ZIF possesses the smallest energetic barriers for electron transfer between reaction adsorbates/intermediates and active sites on the catalyst.[108] MXenes, such as Ti_2CT_2, show great promise as catalysts for NRR, with the catalytic performance being significantly influenced by the functional groups present on the surface. By tuning the surface composition of defective Ti_2CT_2, a series of MXene catalysts with various theoretical work functions can be obtained, such as $Ti_2C(OH)_2$ (2.03 eV), Ti_2CH_2 (4.21 eV), Ti_2CF_2 (4.80 eV), and Ti_2CO_2 (5.61 eV). Further analysis finds a linear-correlation relationship between the ΔG of NRR potential-determining steps and the work function of the four catalysts.[109]

Another important method for regulating composition is through alloying.[76] Alloys comprising two or more metal species are commonly employed as electrocatalysts due to their high activity, good conductivity, etc. In AgAu alloys with various Ag/Au ratios utilized for CO_2RR, the work functions, which are dependent on the Ag content, exhibit a negative correlation with the H_2 partial current densities and a nearly positive correlation with the CO partial current densities (except the bare Ag sample). The $Au_{20}Ag_{80}$ sample with the smallest work function exhibits the highest H_2 evolution performance, while the $Au_{80}Ag_{20}$ sample exhibits the highest CO Faradaic efficiency.[11] Introducing metals with low work function into noble metals (such as Pt) can not only regulate the electronic property but also improve the utilization efficiency of precious metals.[77] In the Pt-PdCu alloy, the difference in the work function of Pt (5.65 eV) and Cu (4.65 eV) triggers the downshift of the *d*-band center of Pt. This regulation of electronic structure can lessen the CO adsorption energy on Pt sites and promote the cleavage of C–H bonds, ultimately improving the catalytic activity toward formic acid/methanol electrooxidation.[110]

4.2.6. Atomic Metal Catalyst Design

The design of SACs and DACs for electrocatalysis attracts growing interest due to the high catalytic activity and efficient utilization of metal atoms.[83,111] Constructing active single-atom metal sites onto substrates would alter the work function of metal catalysts. In the nickel(II) 2,9,16,23-tetra(amino)phthalocyanine (Ni-TAPc)/CNTs, the attachment of Ni-TAPc onto CNTs leads to a decreased work function (from 4.8 to 4.2 eV), suggesting that electrons flow toward NiN_4 after Ni SAC formation. Such an enhanced charge transfer process benefits the following CO_2RR activity and selectivity.[112] In the Ni/MoS_2[113] and Fe/N-doped C[82] catalysts, the formation of metal SACs can help reduce the work function of bare supports, thereby accelerating the catalytic process. When designing a bifunctional catalyst for OER/ORR, Guan and co-authors anchored transition metal single atoms onto tetracoordinated phosphorus-modified graphene (TMP4).[114] There is a positive correlation between the bifunctional catalytic activity and the work function, with larger work functions leading to improved bifunctional catalytic performance. The optimal CoP4 catalyst takes advantage of the hybridization between Co-*d* and *p* orbitals of O-containing groups, possessing the best OER/ORR bifunctional activity. Different from other studies that analyze the relationship between work function and ORR or OER separately,[97] this computational work directly links the OER/ORR bifunctional activity with work function. The conclusion presented in this study might promote the work function-guided design of OER/ORR bifunctional catalysts.

4.2.7. Nanostructure Control

The work function of metal catalysts is sensitive to their nanostructure, making nanostructure control an effective method to adjust the work function of catalysts. For instance, the work functions of transition metal dichalcogenide (like WSe_2, $MoSe_2$, WS_2, and MoS_2) monolayers are ≈0.3 eV higher than those of their nanoribbons.[78] The nanostructure-dependent work function thus guides the design of nanostructured catalysts with high performance. In 2020, Xiao and co-authors developed a hexagonal Zn nanoplates catalyst (H–Zn–NPs) with an electrodeposition-electrochemical reduction method (**Figure 9a**).[115] Compared with Zn foil and similarly sized Zn nanoparticles (S–Zn–NPs), H-Zn-NPs have a lower work function of 3.66 eV (Figure 9b). Therefore, H-Zn-NPs possess a faster electron transfer process and accelerate the reduction of adsorbed CO_2 into the $CO_2^{\bullet-}$ intermediate, which consequently contributes to improved CO_2RR activity (Figure 9c). Further computational results imply that an increasing edge-to-corner ratio would enhance the CO_2RR activity and selectivity (Figure 9d). This principle is feasible for guiding efficient catalyst design with controlled nanostructures and suitable work functions.

During electrochemical reactions, catalysts often undergo in situ structural evolution. This process can alter the work function

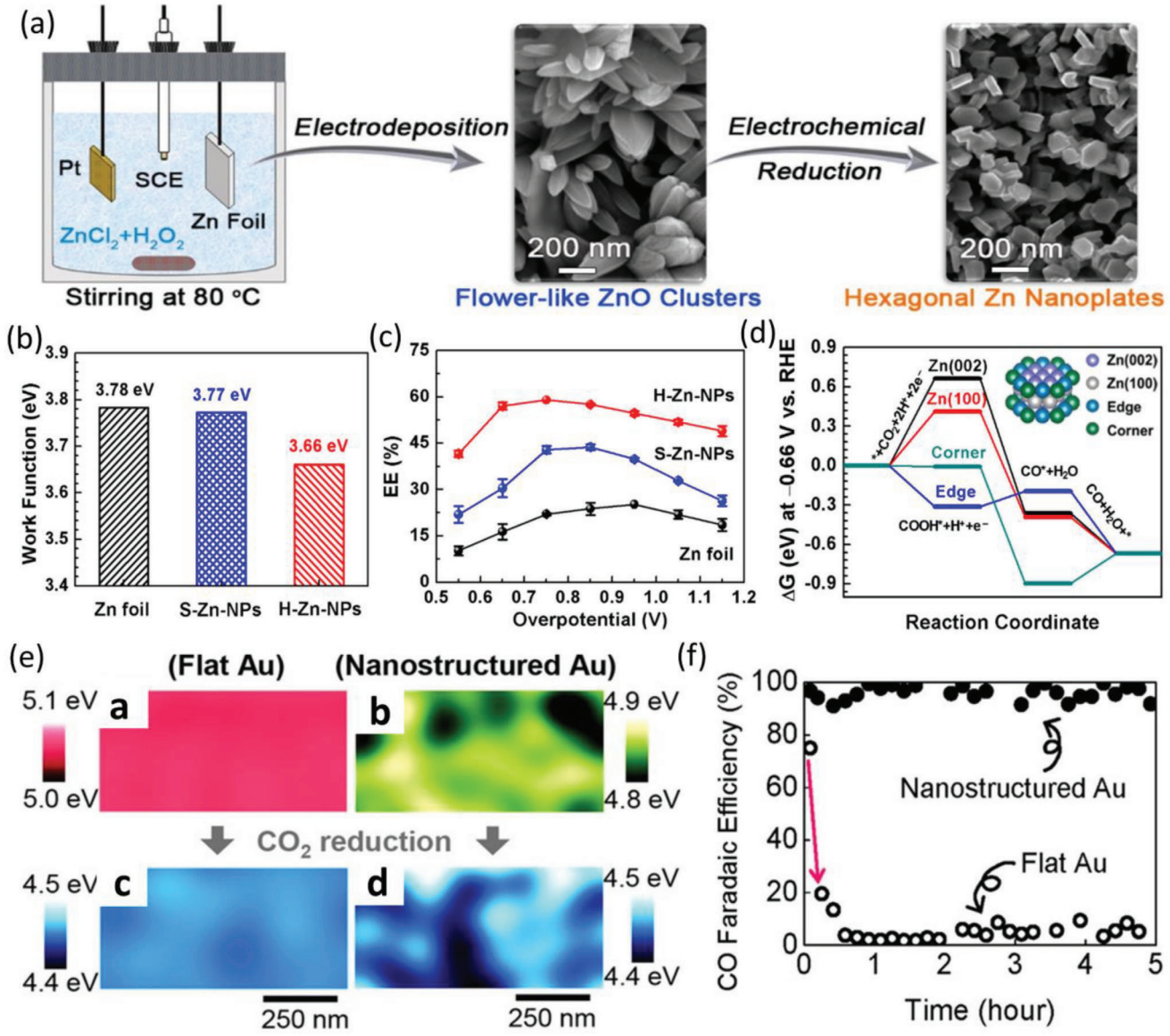

Figure 9. a) Illustration of the synthesis of H-Zn-NPs. b) Work functions of H-Zn-NPs, S-Zn-NPs, and Zn foil. c) Energy efficiency for CO_2-to-CO conversion of H-Zn-NPs, S-Zn-NPs, and Zn foil. d) Free energy profiles for CO_2-to-CO conversion on Zn(100), Zn(002), and corner and edge sites. Reprinted with permission.[115] Copyright 2020, American Chemical Society. e) KPFM images of nanostructured and flat Au electrodes before (pink and green colors) and after (blue colors) CO_2RR (a, flat Au electrode before CO_2RR; b, nanostructured Au electrode before CO_2RR; c, flat Au electrode after CO_2RR; d: nanostructured Au electrode after CO_2RR). f) CO_2 reduction activities of nanostructured Au (•) and flat Au (○) electrodes. Reprinted with permission.[12] Copyright 2016, Wiley-VCH.

of catalysts, and how the nanostructure-dependent work function evolution has gained attention.[116] Kim et al. found that the surface work function of the nanostructured Au electrode was lower than the flat counterpart (Figure 9e). After the electrochemical CO_2 reduction process, the surface work functions of nanostructured and flat Au electrodes are reduced by different degrees.[12] In situ evolution of surface work functions is ascribed to the deposition of chemical impurities with lower work functions (e.g., K, C) on electrode surfaces during CO_2RR. Compared with the nanostructured Au electrode, flat Au shows a higher variation. Thus, the nanostructured Au with lower impurity deposits not only has better CO_2-to-CO conversion activities but also shows enhanced stability by hindering the impurities-induced deactivation (Figure 9f).

The work function-catalytic stability relationship has also been analyzed in the AgCu alloy systems. The Ag-shell structured GD-$Ag_{45}Cu_{55}$ catalyst (GD: galvanic displacement), with a higher work function compared to the porous DE-$Ag_{25}Cu_{75}$ catalyst (DE: dealloying), is more effective in maintaining its surface electronic properties and can protect the exposed metallic Ag from etching. This enhances the ORR stability in the alkaline solution.[117] Besides constructing nanostructures, limiting the size of catalysts is another strategy to reduce the work function. From Ni nanoparticles (14.3 nm) to Ni single-atom catalysts (SACs), the work

function decreased from 5.8 to 5.5 eV. Correspondingly, the Ni SACs with a lower work function possess better CO_2 reduction performance, and a high CO product Faradaic efficiency of 97% is obtained at −0.8 V.[118]

4.2.8. Composite Construction

Constructing metal-based composites is another powerful method to regulate the work function of catalysts.[119] Importantly, different from the material-material IET-mediated heterostructure design discussed in the next section, the metal-based composites mentioned here illustrate the effectiveness of constructing composites in adjusting the work function of catalysts and affecting the material-electrolyte IET in the catalytic process. In other words, such metal-based composites are considered as a whole (monolithic) and only the material-electrolyte IET is considered in their electrocatalytic applications, though they may be composed of multiphase chemically. Recently, hybridizing metal materials with carbon has been developed to produce composites with a lower work function than the parent materials, which contributes to a higher catalytic activity, e.g., $FeSe_2$-$MoSe_2$/rGO,[81] FeNi@NG/NCM@MoS_2 (NG: N-doped graphene, NCM: N-doped carbon matrix),[120] CoFe@NDC@MoS_2 (NDC: N-doped carbon),[48] Ir@S-C/rGO (S-C: sulfur-doped carbon),[121] defective carbon-CoP,[80] Co_4N@d-NCNWs/D (d-NCNWs/D: N-doped carbon nanowalls/diamond),[122] Co@C,[123] and Cu@NCNT/Co_xO_y (NCNT: N-doped CNT).[124] Such a monotonous trend significantly simplifies the design of high-performance metal/carbon composite catalysts, with a procedure to select suitable carbon and metal materials that can form heterostructures with low work functions. Nevertheless, the study by Wu et al. suggested that the Co/carbon composites with a similar work function to that of Pt (5.65 eV) possessed the best ORR performance.[13] In their work, a series of peanut shell-derived S-doped graphitic carbon (bio-C)/cobalt compounds catalysts were designed. The work functions of CoOP@bio-C (CoOP: Co_3O_4 and $Co(PO_3)_2$), Co_3O_4@bio-C, $Co(PO_3)_2$@bio-C, and bio-C-800 are 5.42, 8.35, 6.61, and 5.02 eV, respectively. The work function of CoOP@bio-C is close to that of Pt, which contributes a better ORR activity than its analogs. Further analysis implies that CoOP@bio-C with a suitable work function has good adsorption ability to O_2 and desorption capacity to reaction intermediates, e.g., *OH and*O, thereby leading to enhanced performance.

Overall, by tuning the work function of metal-based catalysts, the material-electrolyte IET can be regulated, and thus catalytic performance is optimized. Strategies like defect engineering, nanostructure control, strain engineering, heteroatom doping, facet engineering, chemical component regulation, and atomic metal catalyst design, and composite construction are effective for altering work functions. Generally, a reduced work function would benefit the catalytic reaction and enhance the catalytic performance. Nevertheless, there are some exceptions, for example, the increased work function leads to better OER catalytic performance over some catalysts,[28,104a,125] and a Pt-like work function contributes to better ORR[13] or HER performance.[50] In these examples, the work function-catalytic performance relationship is established based on the adsorption strength of reaction intermediates. Tsai et al. found that Al-doping could increase the work function of $FeCoNi_2$ and upshift the *d* band center, which leads to optimized binding energies of metal–O* intermediates during OER.[104a] In this context, it is necessary to check the work function-catalytic performance correlation over different types of catalysts on a case-by-case basis for various reactions. Another issue should be raised here is that many studies simultaneously used two or more listed methods to increase the catalytic performance of metal materials (such as nanostructure control/composition regulation,[110] nanostructure control/doping[69]), while the contribution of the individual method to the regulated work function and thus the catalytic performance has not been fully illustrated.

5. Work Function-Regulated Material-Material IET for Heterostructural Catalyst Design

Heterostructures integrating two or more phases into one catalyst take advantage of populated active sites and optimized electronic properties. The difference in work functions of various phases can realize charge transfer and create local electron relocation at the interface, which plays a vital role in optimizing the electronic structure of heterostructures. By coupling components with suitable work functions, diverse heterostructures have been designed for electrochemical energy conversion reactions (**Table 3**). Unlike the work function-guided monolithic catalyst design that focuses on the work function-regulated material-electrolyte IET, the work function-guided heterostructure design discussed here emphasizes the work function-mediated IET between two components in heterostructures.

5.1. Carbon-Based Heterostructures

Carbon materials (e.g., CNTs, graphene, porous nanocarbon) with high surface area and high electronic conductivity are important components in designing heterostructural electrocatalysts. Combining carbon materials with other electroactive materials is a powerful method to construct high-performance heterostructural catalysts.[146] Recently, both carbon/carbon and carbon/metal hybrids have been developed, and the IET between carbon and other components is crucial for the design of efficient heterostructures for electrocatalysis.

5.1.1. Carbon/Carbon Heterostructures

Metal-free electrocatalysts composed of carbon-based composites attract great interest for their eco-friendliness and high activity. The hexagonal boron nitride/reduced graphene oxide (*h*-BN/rGO)[147] and two-dimensional covalent organic frameworks (2D-COFs)/CNTs[148] were developed for OER and OER/ORR, respectively. In these attempts, the incorporation of carbon materials (i.e., rGO and CNTs) can significantly regulate the work function of heterostructural catalysts due to the material-material IET. In the *h*-BN/rGO vdW heterostructure, the work functions of *h*-BN/rGO, rGO, and *h*-BN are 7.48, 7.26, and 6 eV, respectively. Thus, the hybridization of rGO and *h*-BN disturbs the charge

Table 3. A summary of work function (Φ)-guided design of heterostructural catalysts.

Catalyst	Strategy for heterojunction design	Catalytic reaction	Catalytic performance
Co/Co_2P[126]	Mott–Schottky heterojunction	OER/ORR	ΔE[a]: 0.66 V
MoC/N, P-codoped carbon[127]	Mott–Schottky heterojunction	HER	η_{10}: 175 mV, Tafel slope: 62 mV dec^{-1}
Co@CoO[128]	Mott–Schottky heterojunction	HER	η_{10}: 105 mV, Tafel slope: 53 mV dec^{-1}
Ru NCs/P,O-NiFe LDH[129]	Mott–Schottky heterojunction	OWS[b]	E_{10}[c]: 1.466 V
$Ti@Co_{0.85}Se$[130]	Ohmic contact heterojunction	OER	η_{10}: 500 mV, Tafel slope: 153 mV dec^{-1}
$NiMo/Ni_2P$[18]	Ohmic contact heterojunction	HER	η_{10}: 15 mV, Tafel slope: 29.45 mV dec^{-1}
FeNi-LDH/CoP[131]	*p-n* heterojunction	OER	η_{20}: 231.1 mV, Tafel slope: 33.5 mV dec^{-1}
$CoP\text{-}Nb_2O_5$[132]	*p-n* heterojunction	HER	η_{10}: 69 mV, Tafel slope: 72 mV dec^{-1}
$CuS@MoSe_2$[133]	*p-n* heterojunction	OER	η_{10}: 219 mV, Tafel slope: 77.6 mV dec^{-1}
CoP-CoO[134]	*p-p* heterojunction	OWS	E_{10}: 1.65 V
Fe-doped NiP/NiS[135]	*p-p* heterojunction	OER	η_{10}: 204 mV, Tafel slope: 53.7 mV dec^{-1}
$CoP\text{-}CoS_2$[136]	*n-n* heterojunction	OER	η_{10}: 170 mV, Tafel slope: 39 mV dec^{-1}
$Cu_3(HITP)_2@h\text{-}BN$[137]	*n-n* heterojunction	NRR	NH_3 yield: 146.2 μg h^{-1} mg_{cat}^{-1}, FE: 42.5% (−0.3 V vs RHE)
Ni_2P-CoCH[d][138]	Work function difference optimisation	OWS	E_{10}: 1.53 V
Iron phthalocyanine/GaS[139]	Work function difference optimisation	ORR	J_k[e]: 35.7 mA cm^{-2} (0.85 V vs RHE)
$PdRu\text{-}RuO_2$[19]	Work function difference optimisation	EOR[f]	MA: 2348.5 mA mg^{-1}
$Ru\text{-}Ni_{0.85}Co_{0.15}Se$[140]	Work function difference optimisation	HER	η_{10}: 18.2 mV, Tafel slope: 35.61 mV dec^{-1}
NiP_2/Ni_5P_4[141]	In-plane heterojunction	HER	η_{10}: 30 mV, Tafel slope: 30 mV dec^{-1}
FeP@CoP[20]	In-plane heterojunction	HER	η_{10}: 33 mV, Tafel slope: 36 mV dec^{-1}
$Mo_5N_6\text{-}MoS_2$[142]	In-plane Mott–Schottky heterojunction	HER	η_{10}: 57 mV, Tafel slope: 38.4 mV dec^{-1}
Ni/NiOOH[143]	Nanostructure control	OER	η_0: 0.33 V
SnS_{2-x}/NC[144]	Vacancy engineering	CO_2RR	FE for formate: > 80% (−0.8 to −1.2 V vs RHE)
Ir@S-C/rGO[121]	Doping engineering	OWS	E_{10}: 1.51 V
$V\text{-}Ni_3FeN/Ni$[145]	Doping engineering	OWS	E_{10}: 1.55 V

[a] ΔE, potential gap (ΔE) between E_{j10} for OER and $E_{1/2}$ for ORR; [b] OWS, overall water splitting; [c] E_{10}, applied potential at 10 mA cm^{-2} for water electrolysis; [d] Ni_2P-CoCH, nickel phosphide-cobalt nanowire arrays; [e] J_k, kinetic current density; [f] EOR, ethanol oxidation reaction.

balance at the interface and drives electron transfer from *h*-BN to rGO until the Fermi level reaches equilibrium. This process promotes the OER activity of *h*-BN/rGO via altering the interface charge distribution and transport and forming active interface/sites for the catalytic process.[147]

5.1.2. Carbon/Metal Heterostructures

Carbon/metal heterostructures leverage the benefits of both carbon (large surface area, conductivity) and metal catalysts (intrinsic activity), resulting in improved catalytic activity.[149] The carbon-metal IET benefits the optimization of electronic properties of as-formed heterostructures.[124,150] For example, in an N-doped graphene/Co hybrid, the strong chemical coupling between *p*-orbitals of N and C atoms in N-doped graphene and *d*-orbitals of Co atoms helps to tune the adsorption of ORR intermediates and therefore benefits the ORR activity.[151] Finely regulating the work function of the carbon and/or metal components in composites can optimize the catalytic performance. Typically, N-doped carbon is used as a support because the incorporation of N can alter the work function of carbon (such as graphene, CNTs, and porous carbon), which further influences the electronic metal–support interaction (EMSI) between nitrogen-doped carbon and anchored metals. The EMSI has a huge influence on both the activity and stability of catalysts. Lin and co-workers noticed that the graphitic N-doped carbon nanosheets (NGC) with a higher work function than the graphitic carbon (GC) could help suppress the dissolution of supported Pt particles and thus augment the ORR stability (**Figure 10a**).[152] After loading Pt particles, the lower Fermi level of NGC improves electron transfer from Pt to NGC, thereby changing the electronic properties of the composite. As shown in Figure 10b, the *p*-band center of C positively shifted from −8.82 eV (NGC) to −7.67 eV (Pt/NGC), indicating the acceptance of electrons by NGC. In the differential charge density profile, the inner region of Pt exhibits evident electron loss, which is obtained by the NGC support (Figure 10c). Besides regulating the electronic structure of interface Pt, the strong EMSI also reduces the electron density of the outface Pt by the long-range charging of electronic equilibration (Figure 10d). The electron-deficiency feature of the outface can help decrease the Pt–O dipole effect, which is important for keeping the stability of the Pt catalyst. Oxygen temperature-programmed desorption (TPD) results further verify the weaker dipole effect between O_2 and Pt in Pt/NGC than that in Pt/GC (Figure 10e). Compared with the Pt/GC and commercial Pt/C (20%) catalysts, Pt/NGC shows negligible activity loss, low Pt dissolution, and small degradation in kinetic current density (Figure 10f–h). By regulating the work function of carbon substrates, one can control the EMSI and thus improve the stability/activity of carbon/metal catalysts.

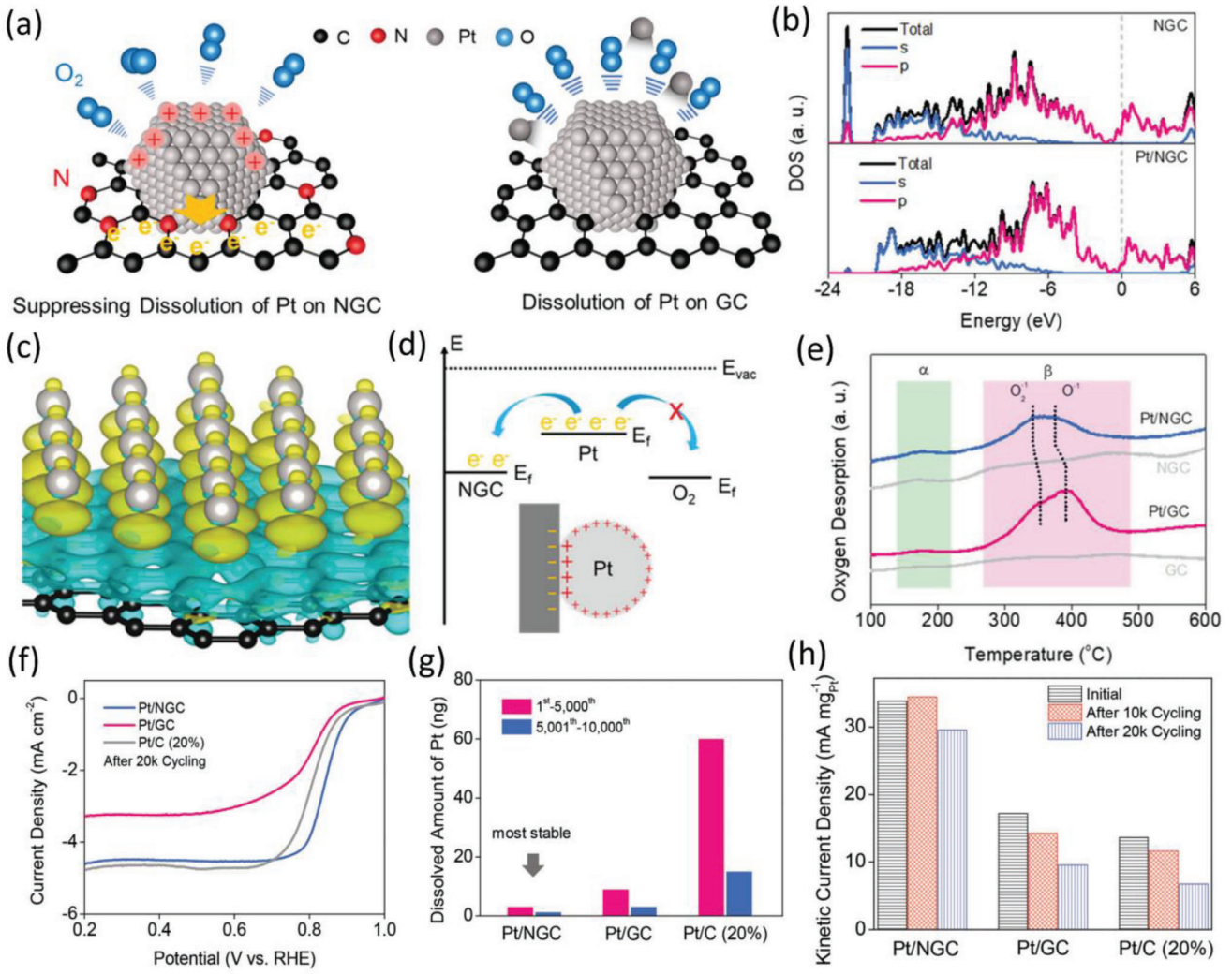

Figure 10. a) Scheme of GC and NGC substrates influencing the Pt–O interaction. b) DOS of C orbitals in Pt/NGC and NGC. c) Differential charge density of Pt/NGC. Blue and yellow regions mean electron accumulation and depletion, respectively. d) Schematic of EMSI between NGC and Pt. e) O_2-TPD results of GC, NGC, Pt/GC, and Pt/NGC. f) ORR LSV curves of Pt/C (20%), Pt/GC, and Pt/NGC after 20k cycling. g) Leached amount of Pt during stability tests. h) Comparison of kinetic current densities for catalysts (0.85 V vs RHE). Reprinted with permission.[152] Copyright 2021, Wiley-VCH.

Chemically modifying metal components (e.g., introduction of vacancy, lattice strain, chemical composition regulation) is an efficient way to tune the metal-carbon IET in carbon/metal composites. Guided by DFT calculations, Li and coauthors loaded the S-deficient SnS_2 on N-doped hollow carbon spheres (SnS_{2-x}/NHCS) toward CO_2RR.[144] As depicted in **Figure 11a**, the work functions of N-doped carbon (represents NHCS), SnS_{2-x}, and SnS_2 are 3.51 eV, 4.04 and 4.19 eV, respectively. Thus, the coupling between N-doped carbon and SnS_{2-x} would trigger electron transfer from the former to the latter, as illustrated by the charge density difference result in Figure 11b,c. This charge redistribution and transfer process enhances the CO_2 adsorption and bonding capabilities of SnS_{2-x}/NHCS compared to the counterparts (Figure 11d,e). This leads to a high local CO_2 concentration, ultimately promoting CO_2-to-carbonaceous product conversion. In the CO_2RR energy profile, SnS_{2-x}/N-doped carbon shows improved bonding with the *OOCH intermediate at the transient state, and the energy barrier for the generation of CO_2* over SnS_{2-x}/N-doped carbon (0.65 eV) is smaller than that over SnS_{2-x} (0.80 eV) and SnS_2 (0.83 eV) (Figure 11f). The largely decreased energy barrier on SnS_{2-x}/N-doped carbon thus accelerates CO_2 activation and conversion processes. By integrating heteroatom doping and defect construction to control the work function of materials, it is efficient to engineer carbon/metal composites with favorable catalytic properties (e.g., adsorption/desorption of reactants and intermediates).

In carbon-based heterostructures, the IET of carbon-carbon and carbon-metal promotes the interfacial interaction and helps to shape the electronic properties of the as-formed heterostructures. Thus, carbon is not only a conductive substrate but also an electronic property modifier in electrocatalysts. By finely adjusting the work function of carbon and/or metal components through techniques such as heteroatom doping and creating

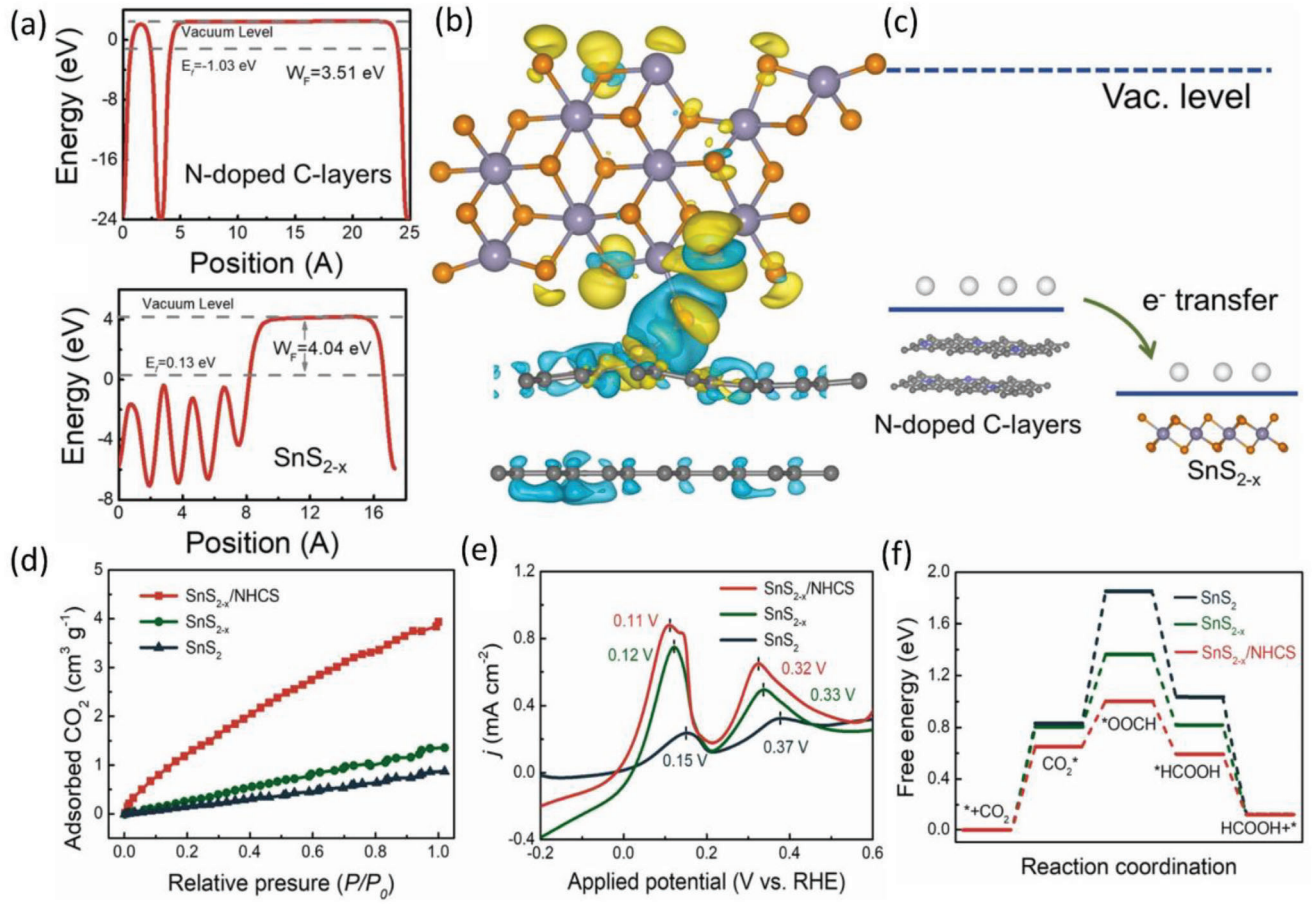

Figure 11. Work function diagrams of a) N-doped carbon and b) SnS_{2-x}. c) Charge density difference image of SnS_{2-x}/N-doped carbon (isosurface value: 1×10^{-3} e Å^{-3}). c) Illustration of the electron transfer process between N-doped carbon and SnS_{2-x}. d) CO_2 adsorption isotherms. e) OH^- adsorption results. f) CO_2RR free energy diagrams for formate generation over SnS_{2-x}/N-doped carbon, SnS_{2-x}, and SnS_2. Reprinted with permission.[144] Copyright 2023, Elsevier.

vacancies, it is possible to optimize the carbon-carbon or carbon-metal interaction and enhance catalytic performance.

5.2. Metal-Based Heterostructures

Heterostructures consisting of two or more metal materials benefit from the material-material IET and the resulting built-in electric field. By integrating metal materials (e.g., metal nanoparticles, alloys, (hydr)oxides, chalcogenides, and pnictides) with different work functions into a composite, a variety of efficient catalysts have been designed for energy conversion reactions.[153] Due to the high flexibility in the work functions and electronic structures of metal materials, the work function-guided design of metal materials-based heterostructures shows some features that are elaborated in this part.

5.2.1. Mott–Schottky Heterojunction

Considering the wide applications of metals (or metallic materials, e.g., alloys, metal sulfides, borides, carbides) and semiconductors (such as metal oxides) in electrocatalysis, diverse metal (metallic material)-semiconductor hybrids have been designed. The interfacial interaction between semiconductors and metals is mainly dictated by their work functions. As shown in **Figure 12**a,b, two types of Schottky junctions can be formed based on the relative work functions of semiconductors and metals.[27b] When the semiconductor work function is smaller than that of the metal, the IET induces an electron-depletion region on the semiconductor side and an electron-rich region on the metal side. As a result of the electron transfer process at the interface, the semiconductor's conduction and valence bands are shifted up, and the semiconductor's Fermi level is shifted down. Of note, the electron deficiency on the semiconductor side decreases gradually from the interface with the metal into the bulk of the semiconductor.

In Mott–Schottky contacts, the built-in electric field with electron–depletion and electron-rich regions formed at the metal/semiconductor interface can significantly regulate the activation/adsorption behavior of reactants/intermediates in electrocatalytic reactions, leading to elevated catalytic performance.[154] To date, hundreds of Mott–Schottky heterojunctions have been developed for diverse electrocatalytic reactions, such as CoP/Co-N-C (for ORR/OER),[17] ReS_2/NiS (for HER),[155] Co/CoP

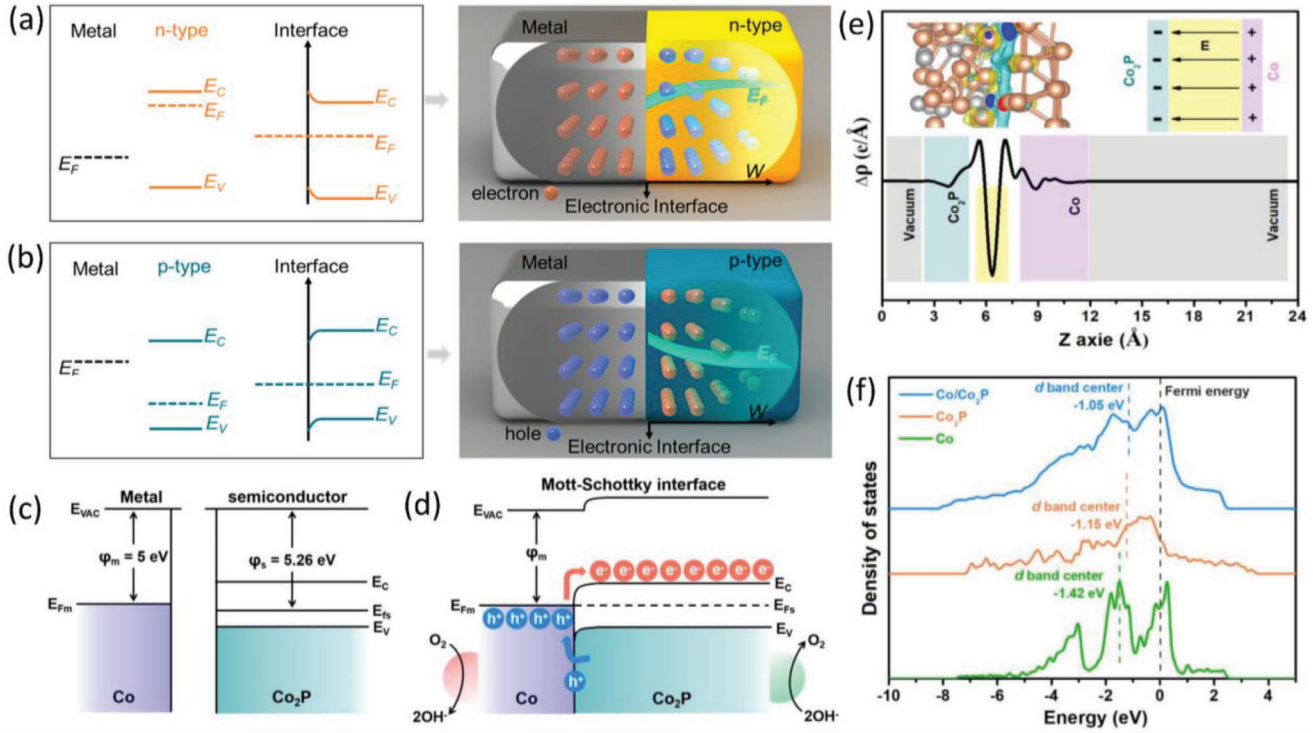

Figure 12. a) Band structures of Mott–Schottky contacts between metals and a) n-type and b) p-type semiconductors (E_C: conduction band, E_V: valence band, E_F: Fermi level). Reprinted with permission.[27b] Copyright 2023, American Chemical Society. c) Band structures of Co and Co_2P. d) Band structures of Co and Co_2P after Schottky contact. e) Charge density difference of the Co/Co_2P Mott–Schottky heterojunction. Insert shows the Co/Co_2P model and the scheme of the built-in electric field. f) Calculated DOS of Co_2P, Co, and Co/Co_2P. Reprinted with permission.[126] Copyright 2021, Elsevier.

(for HER/OER),[156] NiS/MoS_2 (for UOR),[157] Mo_3P/Mo (for CO_2RR),[158] and Co@TiO_2 for (NO_3RR).[159] In the most widely studied metal/metal phosphide heterostructures (e.g., Co/Co_2P), the Schottky contact of Co with Co_2P makes the valence and conduction bands of Co_2P bent downwardly (Figure 12c,d).[126] The spontaneous electron transfer from Co (work function: 5 eV) to Co_2P (work function: 5.26 eV) across the interface establishes a built-in electric field, which provides an electron flow highway and bolsters the utilization efficiency of electroactive sites. The built-in electric fields in Co/Co_2P induced by the Mott–Schottky effect are also evidenced by the charge density difference results in Figure 12e, charges on the Co_2P side (in yellow) are enriched and charges on Co (in cyan and blue) are diminished. The increased electron density on Co_2P helps reduce the energy barrier for adsorption/desorption of reaction intermediates, thereby improving the ORR/OER catalytic kinetics. Also, the electron-deficient Co side can stabilize reaction intermediates (e.g., *O) and enhance the catalytic performance. From the calculated density of state (DOS) results, it can be seen Co/Co_2P shows an upshifted *d*-band center which benefits the adsorption of intermediates during the catalytic process (Figure 12f).

5.2.2. Ohmic Contact Heterojunction

Besides Mott–Schottky heterojunctions, Ohmic contact is another form of interfacial interaction between metals and semiconductors. A main feature of Ohmic contact is that there are no Schottky barriers at the interface (**Figure 13a**).[27b] The Ohmic contact allows electrons to flow freely across the interface without generating any charge spaces on either side. The formation of Ohmic contacts can enhance electron transfer, decrease resistance, and accelerate reactions in electrocatalysis. Recently, Ohmic contact heterojunctions like Ti@$Co_{0.85}Se$,[130] WO_3@W,[160] and NiMo/Ni_2P[18] have been designed for electrocatalytic reactions. Yang and co-authors developed a bifunctional NiMo/Ni_2P hierarchical Ohmic contact heterojunction for overall hydrazine electrolysis, which attains 0.5 A cm^{-2} at only 0.343 V (Figure 13b).[18] The Ohmic contact of NiMo alloy (work function: 4.12 eV) with Ni_2P semiconductor (work function: 4.52 eV) was characterized by *I–V* curve measurements. The hybridization of NiMo and Ni_2P induces charge redistribution and energy band bending at the interface (Figure 13c). The accumulated electrons on the interface can decrease the resistance of the surface and create an electron transfer pathway with a low barrier in any direction, by avoiding the influence of the rectification effect. Through the integration of Ni_2P (active for hydrazine oxidation reaction (HzOR)) and NiMo (active for HER) at the Ohmic contact interface, the NiMo/Ni_2P composite realizes bifunctionality (Figure 13d). In Figure 13e, charges are concentrated at the interface, confirming the transfer of charges from NiMo to Ni_2P and their accumulation at the interface. The electron regulation at the interface optimizes the Gibbs free energy of HER and HzOR, thus reducing the energy barriers of catalytic reactions. Especially, the moderate adsorption strength of reaction intermediates and the facilitated

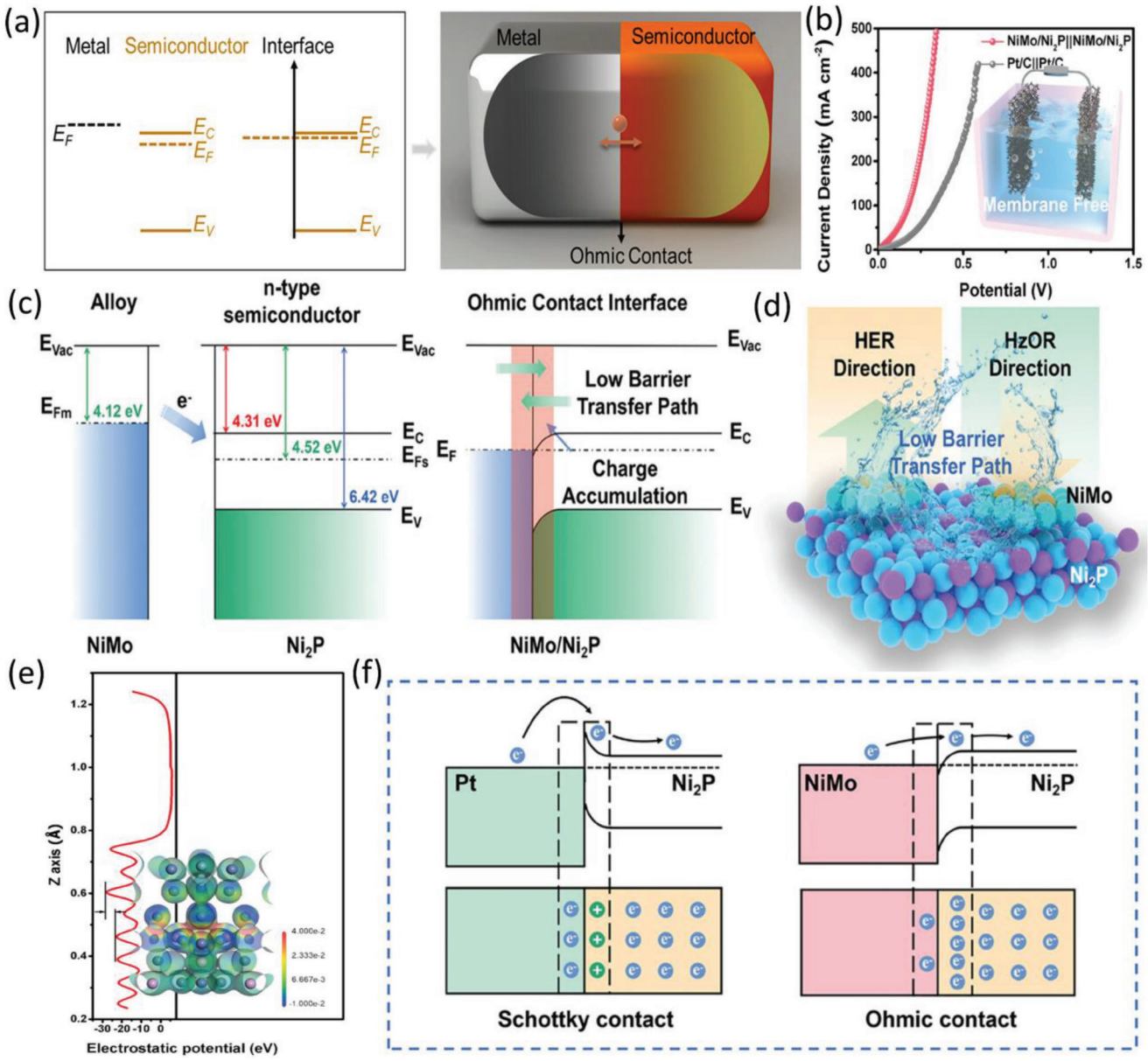

Figure 13. a) Band structures of Ohmic contacts between metals and semiconductors, and corresponding real-space electron transfer illustration. Reprinted with permission.[27b] Copyright 2023, American Chemical Society. b) LSV curves of Pt/C and NiMo/Ni_2P for hydrazine electrolysis. c) Energy band profiles of Ni_2P and NiMo before and after contact. d) Illustration of electrocatalytic reactions on the Ohmic contact interface. e) Electrostatic potential distribution and charge density difference profile of the NiMo/Ni_2P Ohmic contact heterojunction. f) Energy band diagram difference between Ohmic contact and Schottky contact. Reprinted with permission.[18] Copyright 2024, Wiley-VCH.

dehydrogenation process benefit HzOR activity, and the near-zero ΔG_{H^*} promotes the HER performance. In conventional Schottky heterojunctions (e.g., Pt/Ni_2P, Figure 13f), the catalytic performance can be affected by the electric field present at the interface. Importantly, the direction of electron transfer determines the influence of the built-in electric field. When the built-in electric field opposes electron flow, an energy barrier for electron transfer is created, leading to additional energy loss, just like the limited HzOR performance of Pt/Ni_2P. In this context, the NiMo/Ni_2P Ohmic contact without rectification effect could provide a bidirectional electron movement channel with a low energy barrier, thus holding great promise for designing bifunctional catalysts.

5.2.3. p-n, p-p, and n-n Heterojunction

The semiconductor-semiconductor contact emerges as an efficient route to construct heterostructures for electrocatalysts.[133,161] Depending on the band properties of semiconductors, *p-p*,[134–135] *p-n*,[131,133,162] and *n-n*[136–137] heterojunctions have been reported, and both work function and band

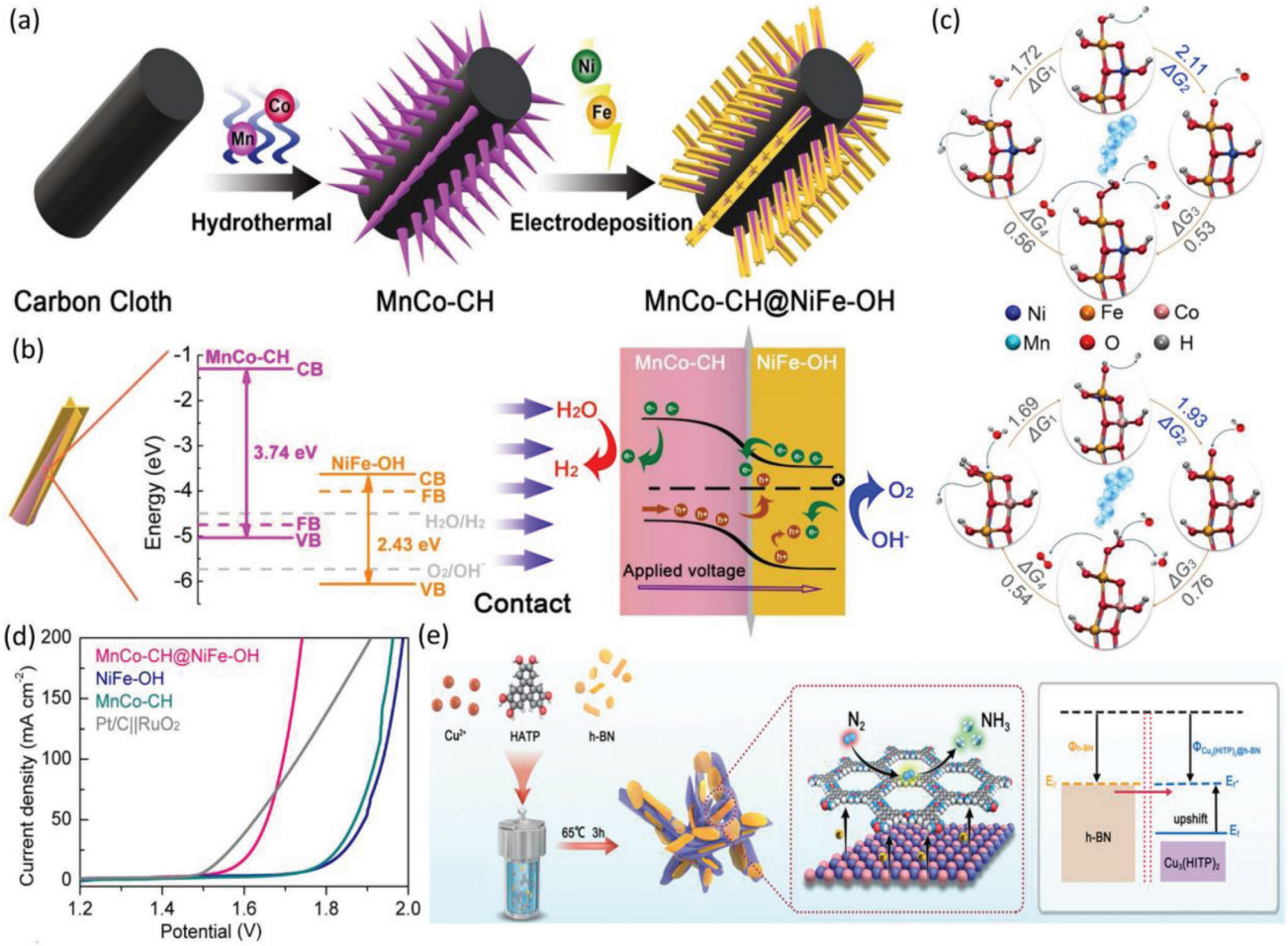

Figure 14. a) Illustration of the synthesis of MnCo-CH@NiFe-OH *p-n* junction. b) Band energy profiles of (left) NiFe-OH and MnCo-CH, and (right) MnCo-CH@NiFe-OH *p-n* junction. c) OER free energy diagrams over (upper) NiFe-OH and (down) MnCo-CH@NiFe-OH. d) Polarization curves of catalysts for overall water electrolysis. Reprinted with permission.[163] Copyright 2021, Elsevier. e) Scheme of the fabrication and application of $Cu_3(HITP)_2$@h-BN *n-n* heterojunction. Reprinted with permission.[137] Copyright 2023, Wiley-VCH.

structure (positions) guide the design process. Different from metal-semiconductor contact, semiconductor-semiconductor junction can benefit from the significantly regulated band properties on both sides of the interface and offer more possibilities to adjust the electron densities of as-formed heterostructural catalysts.[131] The contact of two semiconductors would lead to electron flow and band bending because of the difference in their Fermi level. As a result, the electric field created by the interface can adjust the electron density of nearby atoms. Furthermore, the charged surface profoundly impacts charge transfer and reactant/intermediate adsorption during electrocatalysis.[131] In a typical *p-n* junction MnCo carbonate hydroxide@NiFe oxyhydroxide (MnCo-CH@NiFe-OH) prepared with the hydrothermal process-electrodeposition method (**Figure 14a**), the combination of *p*-type MnCo-CH (work function: 4.75 eV) and *n*-type NiFe-OH (work function: 4.01 eV) leads to the electron transfer from NiFe-OH to MnCo-CH (Figure 14b).[163] The subsequent band bending widens the gap between the theoretical OER potential and the E_{VB} of NiFe-OH. Thus, a positively charged NiFe-OH surface promotes the transport and adsorption of OH^- species onto the NiFe-OH surface, finally boosting the OER performance (Figure 14c). Meanwhile, the band bending broadens the gap between the theoretical HER potential and the E_{CB} of MnCo-CH. This process accelerates the migration of electrons, which promotes the conversion of H^+ to H_2. Accordingly, the MnCo-CH@NiFe-OH *p-n* junction could enhance both the OER and HER activities, compared to the individual counterparts. As depicted in Figure 14d, the bifunctional MnCo-CH@NiFe-OH only takes 1.69 V at 100 mA cm^{-2} for water electrolysis. Another feature of the MnCo-CH@NiFe-OH composite is the integration of dual active sites in different phases, namely MnCo-CH for HER and NiFe-OH for OER respectively. Similarly, such a modular design process has been applied for the design of *n-n* $Cu_3(HITP)_2$@h-BN (HITP: 2,3,6,7,10,11-hexaiminotriphenylene) heterojunction towards NRR (Figure 14e).[137] In this composite, h-BN exhibits good N_2 activation ability, while $Cu_3(HITP)_2$ demonstrates high N_2 adsorption capability. Thus, the integration of the dual active sites and the regulated band properties further promotes catalytic performance.

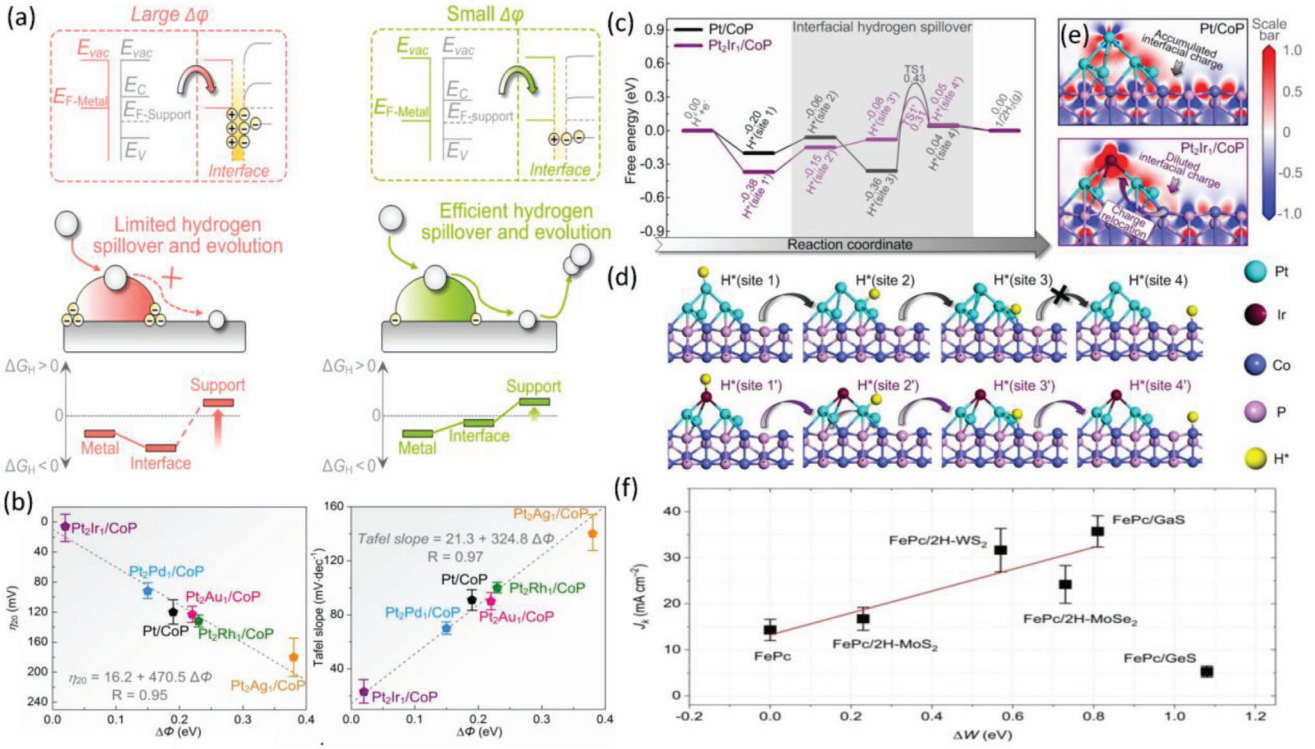

Figure 15. a) Schemes of the interfacial electronic structures and hydrogen spillover phenomena in HER for heterostructural catalysts with (left) large ΔΦ or (right) small ΔΦ. E_C: conduction band, Ev: valence band, E_F: Fermi level, and Evac: vacuum energy. Reprinted with permission.[165] Copyright 2022, American Chemical Society. b) HER activity trends of η_{20} and Tafel slope as a function of ΔΦ. c) Calculated free energy profiles for HER over Pt/CoP and Pt_2Ir_1/CoP catalysts. d) Optimized H* adsorption models on various sites. e) Electron density difference at the interface. Blue: electron loss, red: electron enrichment. Reproduced under terms of the CC-BY license.[166] Copyright 2021, The Authors, published by Springer Nature. f) Kinetic current densities (J_k) at 0.85 V versus RHE, plotted as a function of the work function difference (ΔW) between metal chalcogenides and FePc. Reprinted with permission.[139] Copyright 2023, Wiley-VCH.

Considering the huge diversity in semiconductors' chemical composition and electronic properties, numerous *p-n*, *p-p*, and *n-n* heterojunctions can be developed for electrocatalysis. By selecting semiconductors with suitable work functions and band positions, it is feasible to manipulate the semiconductor-semiconductor IET and refine the electronic properties of heterostructures. The optimization of work function and band position can be assisted by conventional catalyst design strategies, such as heteroatom doping, defect engineering, and chemical composition regulation.

5.2.4. Work Function Difference Optimization

Based on the discussions of metal-semiconductor and semiconductor-semiconductor heterojunctions that link the catalytic activity with the work function values of the metal and semiconductor components in composites, finely turning the work function difference (ΔΦ) between two metal-based materials is thus proposed to optimize the electronic properties of the as-formed heterostructures. The regulation of ΔΦ between two components of the interface can affect the flow of interfacial charges and the relocation of surface charges, resulting in tunable electronic properties at the interface.[164] Does a large or a small ΔΦ benefit the catalytic performance? The answer depends on the target reactions. For HER, several studies suggest that a small ΔΦ is better due to the facilitated hydrogen spillover effect.[19] As illustrated in **Figure 15a**, a large ΔΦ between the two components will lead to electron accumulation at the interface, which would further cause strong reactive hydrogen species (H*) trapping at the interface.[165] This process induces high kinetic barriers for the interfacial hydrogen spillover from one metal component to another phase, thus leading to unsatisfactory HER performance. Conversely, a small ΔΦ could help restrain the IET and minimize the accumulated charge at the interface. As such, the energy barrier for interfacial hydrogen spillover would be largely decreased, theoretically contributing to high HER activities. Li et al. developed a series of PtM (M = Ag, Pd, Au, Rh, and Ir) alloys/CoP composite for HER.[166] It is suggested that the plots of the tested HER activity (η_{20} and Tafel slope) and ΔΦ of the six catalysts show a nearly linear decreasing trend (Figure 15b). The Pt_2Ir_1/CoP with the smallest ΔΦ of 0.02 eV exhibits the highest HER performance. DFT calculations indicate that H* preferentially adsorbed at the Pt site on the Pt/CoP surface, and the ΔG_H values at site 1 (−0.20 eV), site 2 (−0.06 eV), and site 3 (−0.36 eV) imply prominent proton trapping at the interface of CoP and Pt (site 3) (Figure 15c-d). Especially, the robust hydrogen capturing ability at site 3 hinders the hydrogen spillover process. Accordingly, the overall HER process is restrained by the diffusion of

active hydrogen species across the interface from site 3 to site 4 with a large kinetics (0.79 eV) and thermodynamic barrier (0.40 eV). In the Pt_2Ir_1/CoP catalyst, the hydrogen spillover process is significantly facilitated due to the more balanced ΔG_H values over different sites. Further electronic structure analysis suggests that the large $\Delta\Phi$ of Pt and CoP leads to electron accumulation at the interface, and the formed strong bond between the proton and interfacial sites hinders the interfacial hydrogen spillover (Figure 15e). When Ir is introduced into Pt, it causes a significant relocalization of electrons. The diluted electron cloud at the Pt_2Ir_1/CoP interface restrains the IET and minimizes interfacial electron accumulation. The hydrogen adsorption at interface site in Pt_2Ir_1/CoP is thus largely impaired and becomes thermo-neutral, which serves as a mediator for interfacial hydrogen spillover. Therefore, a small $\Delta\Phi$ promotes the interfacial hydrogen spillover process and benefits the HER performance. Similar HER catalyst systems that take advantage of the small $\Delta\Phi$-induced enhanced interfacial hydrogen spillover are also reported in Ru_1Fe_1/CoP,[165] $Ru/Ni_{0.85}Co_{0.15}Se$,[140] and $PdRu/RuO_2$.[19]

Differently, Zhuang and co-authors found that a larger $\Delta\Phi$ between iron phthalocyanine (FePc, *p*-type semiconducting character) and *n*-type metal chalcogenides contributes to a better ORR activity.[139] In such *p-n* hybrids, an approximately linear increase in ORR activity of catalysts as $\Delta\Phi$ (ΔW in this work) increases is noticed, and FePc/GaS with the largest ΔW outperforms others (Figure 15f). Structural characterizations find that the rectification in the composite causes remarkable destabilization of the Fe–N coordination and distortion of the FeN_4 moiety, which also regulates the Fe center's spin configuration and local electron density. Especially, the electron accumulation on the *p*-type FePc generates more unpaired *d* electrons in the Fe^{II} centre, thereby producing more singly occupied and π-symmetry *d* orbitals for O_2 adsorption/dissociation during ORR and higher rectification is attained at higher ΔW. An exception is *p*-type GeS, the hybridization of *p-p* FePc/GeS leads to hole accumulation at the FeN_4 moiety, which is in the opposite direction to that of other *p-n* junctions and thus undermines the ORR activity.

5.2.5. In-Plane Heterostructure Design

The orientation (growth direction) of metal components can impact the work function of composites, thereby influencing the catalytic performance. Recently, in-plane heterostructures have received growing interest.[141–142,167] As suggested, in-plane heterojunctions exhibit different interface electronic interactions from those of conventional vertical heterostructures.[20] In the study by Zhang et al., the in-plane FeP@CoP heterojunction outperformed a vertical counterpart for HER in the whole pH range.[20] To explain the better performance of in-plane FeP@CoP, comprehensive computational studies were performed. In both vertical FeP/CoP and in-plane FeP@CoP models (**Figure 16**a,b), the contact of FeP with CoP leads to electronic structure rearrangement at the interface. However, vertical FeP/CoP shows a significantly lower charge transfer strength than that of in-plane FeP@CoP (Figure 16c). In the in-plane FeP@CoP, the charge deficiency regions (green color) around Co and Fe atoms are shown, and the charge accumulation is primarily between Co–P and Fe–P bonds at the interfaces (red color). The authors suggested that the neutralized work function rearranged the charge states of the interface. For the vertical FeP/CoP (Figure 16d), when the FeP and CoP interfaces are in contact, electrons would flow from FeP to CoP due to the different Fermi energies until the two Fermi energies reach the same level, thus forming an electron depletion layer. This means that more energy is consumed to balance the Fermi energy level, in contrast to the in-plane CoP@FeP, where the electrons are kept horizontal, which does not require excess electron-balancing Fermi energy (Figure 16e), indicating the inherent superiority of the in-plane structure. Further electrostatic potential analysis indicates a dual center of nucleophilicity (Fe) and electrophilicity (Co) within the in-plane FeP@CoP interface, and the regulated nucleophilic and electrophilic sites transfer electrons from the electrode to HER intermediates and accelerate the reaction kinetics, thus enhancing the intrinsic activity. For the vertical FeP/CoP, the nucleophilic and electrophilic centers are separated from each other in an up-and-down manner, limiting the reaction process. As depicted in Figure 16f, the potential determining step (PDS) of vertical FeP/CoP is the H_2O adsorption step, while the PDS of in-plane FeP@CoP is the H_2 production step with a much lower energy barrier (0.27 vs 0.58 eV). The largely facilitated H_2O adsorption/activation over in-plane FeP@CoP is further explained by the crystal orbital Hamiltonian layout (Figure 16g). The hybridization between the 3*d* orbitals of Fe below the Fermi energy level and the orbitals of H_2O molecules promotes the generation of Fe-O bonds, which further accelerates the H_2O activation step. For acidic HER, the in-plane FeP@CoP has near-zero ΔG_{H^*} of −0.02 eV, which is more favorable than Pt (−0.09 eV) and vertical FeP/CoP (0.22 eV) (Figure 16h), implying the best intermediate adsorption/desorption behavior in acidic electrolyte over in-plane FeP@CoP.

By adjusting the growth direction of heterostructures, it is sensible to alter the material-material IET in the catalysts and shape the electronic interaction at the coupling interface. Compared with vertical heterostructures, in-plane ones benefit from the intimate contact of different phases and possess more opportunities for electronic property regulation. Based on current two-phase heterojunctions, the construction of multiphase (three or more phases) in-plane heterostructures is a promising route to precisely navigate the material-material IET and help high-performance catalyst design.

Given the high flexibility in metal species, nanostructures, and electronic properties, metal-based heterostructures are extensively applied for diverse catalytic reactions. For engineering efficient metal-based heterostructures with suitable material-material IET, constructing Mott–Schottky heterojunctions, Ohmic contact heterojunctions, *p-n*/*p-p*/*n-n* heterojunctions, regulating work function difference ($\Delta\Phi$), and designing in-plane heterostructures are promising work function-guided design strategies. Additionally, reducing the size of metal components,[21] introducing dopants/vacancies,[140,168] and decreasing the thickness of metal materials[143] are also capable of tuning the material-material IET for developing metal-based efficient heterostructures. By changing the work functions of single or dual metal components, all of these strategies are effective in tuning the electronic properties of the interface and ultimately promote the catalytic process.

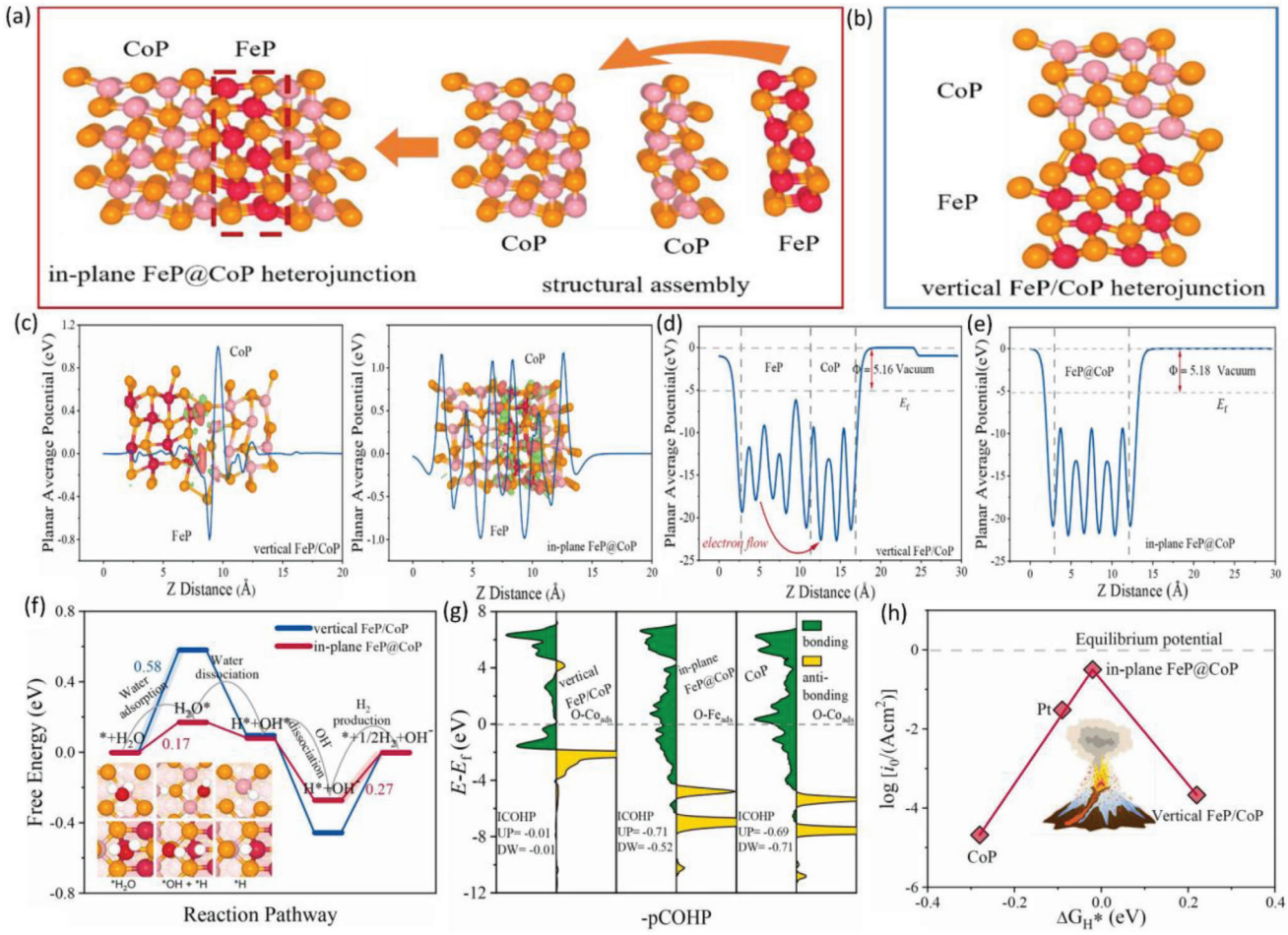

Figure 16. Models of a) in-plane FeP@CoP and b) vertical FeP/CoP. c) Average electron density difference along the Z-axis of in-plane FeP@CoP and vertical FeP/CoP. Work functions of d) vertical FeP/CoP and e) in-plane FeP@CoP heterostructure systems. f) Alkaline HER reaction pathways of vertical FeP/CoP and in-plane FeP@CoP. g) Crystal orbital Hamiltonian population (COHP) of CoP, in-p lane FeP@CoP, and vertical FeP/CoP. h) Relationship of ΔG_{H^*} and exchange current density of different catalysts. Reprinted with permission.[20] Copyright 2023, Elsevier.

6. Conclusions and Perspectives

Designing efficient catalysts for electrochemical energy reactions is critical for accelerating the decarbonization of the global energy sector. As a main electronic property of materials, work function has been employed for catalyst design. In this review, the latest advances in work function-guided electrocatalyst design are summarized, including the work function-based catalytic activity descriptors, monolithic catalyst design, and heterostructure design. By controlling the material-electrolyte IET, the work function works well as a catalytic activity descriptor for different electrochemical catalytic reactions. Based on this, a series of methods have been developed to regulate the work function of monolithic catalysts and thus optimize the catalytic performance. For heterostructure design, efficient strategies (constructing Mott–Schottky heterojunctions, Ohmic contact heterojunctions, *p-n/p-p/n-n* heterojunctions, regulating work function difference ($\Delta\Phi$), and designing in-plane heterostructures) are proposed to regulate the work function-governed material-material IET and achieve efficient heterostructural electrocatalysts. Although significant progress has been made in work function-guided catalyst design, continuous efforts should be devoted to addressing some pressing issues (**Figure 17**).

6.1. Work Function Determination

Accurately measuring the work function of materials lays the foundation of work function-guided catalyst design. This acquires the consistency of sample preparation and standardized testing methods. Instead of analyzing the overall work function of a whole material, developing techniques to analyze the local work function of specific sites can help to identify the catalytically active sites on electrocatalysts. Based on the work function-dependent catalytic activity relationship, it would be a facile route to capture the highly active sites on catalysts by measuring the local work function of typical regions.[89,169] Furthermore, one can characterize the highly active sites and uncover their physicochemical properties (such as chemical composition, shape, and electronic features) for designing high-performance catalysts with dense highly active sites. Notwithstanding computational methods have been widely used to

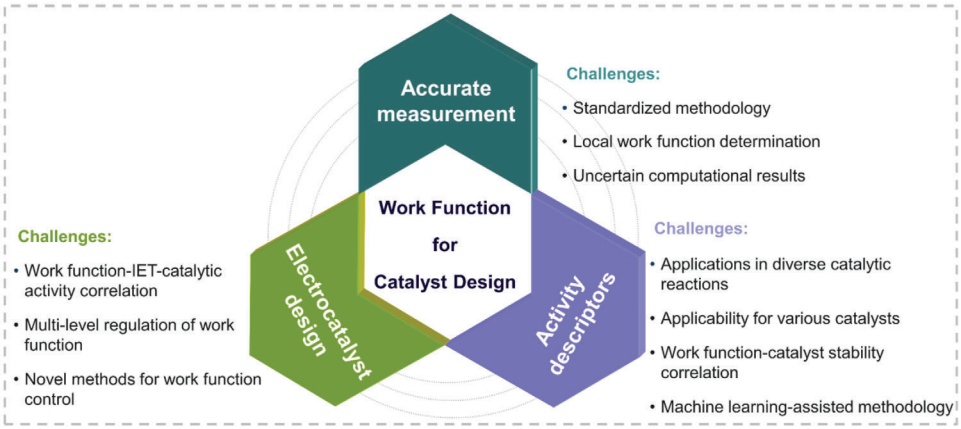

Figure 17. Challenges in work function-guided catalyst design.

determine the work function of materials, the inaccuracy raised by the nanostructure, size, and surface chemistry should be considered.

6.2. Activity Descriptors

Currently, electronic properties-based descriptors like *d* band center, *p* band center, and e_g filling have attracted great attention, and these descriptors significantly promote the development of electrocatalysts for various reactions.[23e] However, these purely computational descriptors may fail to fully elucidate the relationship between catalysts' structure and performance, as the catalytic performance of materials is influenced by factors such as nanostructure, size, crystallinity, and not just their electronic properties. In this regard, the work function, which can be easily determined through experimental methods, is valuable for its broad applicability and high accuracy in analyzing the structure-performance correlation of catalysts with diverse physicochemical properties. Section 3 has discussed current work function-based catalytic descriptors. These descriptors mainly focus on electrochemical reduction reactions, like HER, ORR, CO_2RR, and NRR. Electrooxidation reactions are less explored, although the work function-catalytic activity relationship in the OER and GOR systems has been found in several experimental studies. Another issue is that most available work function-based descriptors are verified based on metal catalysts, while other catalyst systems are rarely investigated. In this context, more efforts are suggested to investigate the work function-adsorption of reactant/intermediate-catalytic activity correlation of catalysts with similar properties (e.g., conductivity, catalyst category). Machine learning-assisted computational methods can further accelerate this process, with the assistance of standardized experimental and computational databases. In addition, most of the current studies have not investigated the work function-stability relationship of electrocatalysts, albeit the work function governed stability of Au electrode in CO_2RR has been pointed out.[12] Analyzing the work function-activity/stability relationship would benefit the development of catalysts with high activity and durability for practical applications.

6.3. Catalyst Design

Guided by the work function-mediated material–electrolyte IET, the design of monolithic catalysts mainly concentrates on optimizing the catalytic performance via regulating catalysts' work function values. In many studies, the relationship between modulated work function and catalytic performance is obtained with only two or three samples, which may lead to arbitrary conclusions. It is highly recommended to design multiple samples to analyze the effects of regulated work function on the catalytic performance. For example, one can use different doping levels in a large range to modulate the work function of materials, and the obtained work function–catalytic performance relationship (liner or volcano-shaped plots) would be more accurate than that derived from the sample with one or two doping levels. For heterostructure design, the work function mediated IET between different components helps form active catalysts. To date, only limited methods have been developed for regulating the IET between different components, as discussed in Section 5. Precise control of the work function of components in heterojunctions is thus hopeful to optimize the overall performance of heterostructures by shaping the material-material IET. By identifying the work function-IET-catalytic performance relationship, it will be convenient for researchers to develop high-performance electrocatalysts. Finally, developing in situ techniques like X-ray absorption spectroscopy, infrared spectroscopy and Raman spectroscopy is crucial for real-time monitoring of catalytic processes. The integration of experimental data with computational results will deepen our comprehension of catalytic mechanisms, providing valuable insights into work function regulation and catalytic performance optimization.

Acknowledgements

This work was supported by the Australian Research Council (DP220101139, DP220101142, DP220100306, and CE230100017). W.-Y. W. thanks the financial support from the RGC Senior Research Fellowship Scheme (SRFS2021-5S01), Research Institute for Smart Energy (CDAQ), and Miss Clarea Au for the Endowed Professorship in Energy (847S).

Open access publishing facilitated by University of New South Wales, as part of the Wiley - University of New South Wales agreement via the Council of Australian University Librarians.

Conflict of Interest

The authors declare no conflict of interest.

Keywords

activity descriptors, electrocatalysts, electrochemical energy conversion, electronic structure, heterostructures, interfacial electron transfer

Received: January 30, 2024
Revised: April 14, 2024
Published online: May 7, 2024

[1] a) F.-Y. Chen, Z.-Y. Wu, S. Gupta, D. J. Rivera, S. V. Lambeets, S. Pecaut, J. Y. T. Kim, P. Zhu, Y. Z. Finfrock, D. M. Meira, *Nat. Nanotechnol.* **2022**, *17*, 759; b) L. Li, P. Wang, Q. Shao, X. Huang, *Adv. Mater.* **2021**, *33*, 2004243; c) G. M. Tomboc, S. Choi, T. Kwon, Y. J. Hwang, K. Lee, *Adv. Mater.* **2020**, *32*, 1908398; d) Z. Chen, R. Zheng, T. Bao, T. Ma, W. Wei, Y. Shen, B.-J. Ni, *Nano-Micro Lett.* **2023**, *15*, 210; e) N. Han, X. Zhang, C. Zhang, S. Feng, W. Zhang, W. Guo, R. Zheng, R. Zheng, P. Liu, Y. Li, J. Fransaer, B.-L. Su, *Matter* **2024**, *7*, 1330.

[2] a) X.-L. Zhang, P.-C. Yu, X.-Z. Su, S.-J. Hu, L. Shi, Y.-H. Wang, P.-P. Yang, F.-Y. Gao, Z.-Z. Wu, L.-P. Chi, Y.-R. Zheng, M.-R. Gao, *Sci. Adv.* **2023**, *9*, eadh2885; b) Z. Chen, N. Han, R. Zheng, Z. Ren, W. Wei, B. J. Ni, *SusMat* **2023**, *3*, 290; c) S.-K. Geng, Y. Zheng, S.-Q. Li, H. Su, X. Zhao, J. Hu, H.-B. Shu, M. Jaroniec, P. Chen, Q.-H. Liu, *Nat. Energy* **2021**, *6*, 904; d) Z. Chen, W. Wei, H. K. Shon, B.-J. Ni, *Green Chem.* **2024**, *26*, 631.

[3] a) S. Jiao, X. Fu, H. Huang, *Adv. Funct. Mater.* **2022**, *32*, 2107651; b) Q. Hu, K. Gao, X. Wang, H. Zheng, J. Cao, L. Mi, Q. Huo, H. Yang, J. Liu, C. He, *Nat. Commun.* **2022**, *13*, 3958.

[4] J. He, T. Zheng, D. Wu, S. Zhang, M. Gu, Q. He, *ACS Catal.* **2022**, *12*, 1601.

[5] a) J. Suntivich, K. J. May, H. A. Gasteiger, J. B. Goodenough, Y. Shao-Horn, *Science* **2011**, *334*, 1383; b) M. Yu, G. Li, C. Fu, E. Liu, K. Manna, E. Budiyanto, Q. Yang, C. Felser, H. Tüysüz, *Angew. Chem., Int. Ed.* **2021**, *60*, 5800.

[6] a) H. Zou, L. Guo, H. Xue, Y. Zhang, X. Shen, X. Liu, P. Wang, X. He, G. Dai, P. Jiang, H. Zheng, B. Zhang, C. Xu, Z. L. Wang, *Nat. Commun.* **2020**, *11*, 2093; b) Y. Zhou, C. Zhang, D. Huang, W. Wang, Y. Zhai, Q. Liang, Y. Yang, S. Tian, H. Luo, D. Qin, *Appl. Catal. B* **2022**, *301*, 120749.

[7] A. R. Zeradjanin, A. Vimalanandan, G. Polymeros, A. A. Topalov, K. J. J. Mayrhofer, M. Rohwerder, *Phys. Chem. Chem. Phys.* **2017**, *19*, 17019.

[8] J. Y. Cheon, J. H. Kim, J. H. Kim, K. C. Goddeti, J. Y. Park, S. H. Joo, *J. Am. Chem. Soc.* **2014**, *136*, 8875.

[9] S. Kumaravel, D. Kumar, S. Sam Sankar, A. Karmakar, R. Madhu, K. Bera, H. N. Dhandapani, S. Nagappan, S. Chakraborty, S. Kundu, *Catal. Sci. Technol.* **2023**, *13*, 694.

[10] S. Sarkar, S. D. Ramarao, T. Das, R. Das, C. P. Vinod, S. Chakraborty, S. C. Peter, *ACS Catal.* **2021**, *11*, 800.

[11] A. M. Ismail, E. Csapó, C. Janáky, *Electrochim. Acta* **2019**, *313*, 171.

[12] H. Kim, H. S. Jeon, M. S. Jee, E. B. Nursanto, J. P. Singh, K. Chae, Y. J. Hwang, B. K. Min, *ChemSusChem* **2016**, *9*, 2097.

[13] Y. Wu, Y. Chen, H. Wang, C. Wang, A. Wang, S. Zhao, X. Li, D. Sun, J. Jiang, *J. Mater. Chem. A* **2018**, *6*, 12018.

[14] M. Li, B. Cai, R. Tian, X. Yu, M. B. H. Breese, X. Chu, Z. Han, S. Li, R. Joshi, A. Vinu, T. Wan, Z. Ao, J. Yi, D. Chu, *Chem. Eng. J.* **2021**, *409*, 128158.

[15] a) Z. Chen, S. Yun, L. Wu, J. Zhang, X. Shi, W. Wei, Y. Liu, R. Zheng, N. Han, B.-J. Ni, *Nano-Micro Lett.* **2023**, *15*, 4; b) T.-F. Li, J. Li, L.-P. Zhang, J.-W. Ke, M.-X. Fan, L.-F. Zhang, C.-W. Deng, Y. Sun, T. Qian, C.-L. Yan, *Rare Met.* **2024**, *43*, 489.

[16] M.-Y. Ma, H.-Z. Yu, L.-M. Deng, L.-Q. Wang, S.-Y. Liu, H. Pan, J.-W. Ren, M. Y. Maximov, F. Hu, S.-J. Peng, *Tungsten* **2023**, *5*, 589.

[17] C. He, Q. Liu, H. Wang, C. Xia, F.-M. Li, W. Guo, B. Y. Xia, *Small* **2023**, *19*, 2207474.

[18] Y. Yang, X. Li, G. Liu, H. Liu, Y. Shi, C. Ye, Z. Fang, M. Ye, J. Shen, *Adv. Mater.* **2024**, *36*, 2307979.

[19] H. Xu, K. Wang, G. He, H. Chen, *J. Mater. Chem. A* **2023**, *11*, 17609.

[20] K. Zhang, J. Jia, E. Yang, S. Qi, H. Tian, J. Chen, J. Li, Y. Lou, Y. Guo, *Nano Energy* **2023**, *114*, 108601.

[21] S.-N. Zhang, P. Gao, L.-H. Sun, J.-S. Chen, X.-H. Li, *Chem. – A Eur. J.* **2022**, *28*, 202103918.

[22] J. Liu, W. Luo, L. Wang, J. Zhang, X.-Z. Fu, J.-L. Luo, *Adv. Funct. Mater.* **2022**, *32*, 2110748.

[23] a) S. Jiao, X. Fu, H. Huang, *Adv. Funct. Mater.* **2022**, *32*, 2107651; b) Z.-J. Zhao, S. Liu, S. Zha, D. Cheng, F. Studt, G. Henkelman, J. Gong, *Nat. Rev. Mater.* **2019**, *4*, 792; c) A. Kumar, Y. Zhang, W. Liu, X. Sun, *Coord. Chem. Rev.* **2020**, *402*, 213047; d) M. Zhang, K. Zhang, X. Ai, X. Liang, Q. Zhang, H. Chen, X. Zou, *Chin. J. Catal.* **2022**, *43*, 2987; e) B. Wang, F. Zhang, *Angew. Chem., Int. Ed.* **2022**, *61*, 202111026; f) Y. Wang, W. Qiu, E. Song, F. Gu, Z. Zheng, X. Zhao, Y. Zhao, J. Liu, W. Zhang, *Kwansei Gakuin Univ. Nat. Sci. Rev.* **2017**, *5*, 327; g) S. D. Bhoyate, J. Kim, F. M. de Souza, J. Lin, E. Lee, A. Kumar, R. K. Gupta, *Coord. Chem. Rev.* **2023**, *474*, 214854; h) J. Zhu, S. Mu, *Inorg. Chem. Front.* **2023**, *10*, 2220.

[24] W. T. Hong, M. Risch, K. A. Stoerzinger, A. Grimaud, J. Suntivich, Y. Shao-Horn, *Energy Environ. Sci.* **2015**, *8*, 1404.

[25] F. Calle-Vallejo, *Adv. Sci.* **2023**, *10*, 2207644.

[26] a) D. S. Baek, J. Lee, J. S. Lim, S. H. Joo, *Mater. Chem. Front.* **2021**, *5*, 4042; b) F. C. Østergaard, A. Bagger, J. Rossmeisl, *Curr. Opin. Electrochem.* **2022**, *35*, 101037.

[27] a) H. Xu, J. Li, X. Chu, *Nanoscale Horiz.* **2023**, *8*, 441; b) D. Xu, S.-N. Zhang, J.-S. Chen, X.-H. Li, *Chem. Rev.* **2023**, *123*, 1; c) H. Xu, J. Li, X. Chu, *Chem. Rec.* **2023**, *23*, 202200244; d) Y. Zhang, Y. Lin, T. Duan, L. Song, *Mater. Today* **2021**, *48*, 115.

[28] H. K. Park, H. Ahn, T. H. Lee, J. Y. Lee, M. G. Lee, S. A. Lee, J. W. Yang, S. J. Kim, S. H. Ahn, S. Y. Kim, C.-H. Lee, E. S. Park, H. W. Jang, *Small Methods* **2021**, *5*, 2000755.

[29] a) J. W. Kim, A. Kim, *Curr. Appl. Phys.* **2021**, *31*, 52; b) L. Zhai, X. She, L. Zhuang, Y. Li, R. Ding, X. Guo, Y. Zhang, Y. Zhu, K. Xu, H. J. Fan, *Angew. Chem., Int. Ed.* **2022**, *134*, 202116057; c) Z. Gu, L. Li, G. Du, Y. Lin, L. Lu, J. Chen, Z. Du, R. Liu, Q. Cheng, K. Gao, *Appl. Phys. Lett.* **2022**, *120*, 123902.

[30] Y. Zhang, W. Yu, H. Zhang, Y. Shi, J. Zhu, T. Wang, Y. Sun, T. Zhan, J. Lai, L. Wang, *Small* **2024**, *20*, 2308440.

[31] R. H. Fowler, L. Nordheim, *Proc. Royal Soc. Lond. A* **1928**, *119*, 173.

[32] X. Li, J. Yu, J. Jia, A. Wang, L. Zhao, T. Xiong, H. Liu, W. Zhou, *Nano Energy* **2019**, *62*, 127.

[33] G. Shao, *Energy Environ. Mater.* **2021**, *4*, 273.

[34] X. Wang, G. Zhang, L. Yang, E. Sharman, J. Jiang, *WIREs Comput. Mol. Sci.* **2018**, *8*, e1369.

[35] Z.-Z. Wu, F.-Y. Gao, M.-R. Gao, *Energy Environ. Sci.* **2021**, *14*, 1121.

[36] T. Liu, C. Xi, C. Dong, C. Cheng, J. Qin, S. Hu, H. Liu, X.-W. Du, *J. Phys. Chem. C* **2019**, *123*, 28319.

[37] R. Cheng, Y. Min, H. Li, C. Fu, *Nano Energy* **2023**, *115*, 108718.

[38] a) L. Lin, R. Jacobs, T. Ma, D. Chen, J. Booske, D. Morgan, *Phys. Rev. Appl.* **2023**, *19*, 037001; b) L. Tao, Y. Wang, Y. Zou, N. Zhang, Y. Zhang, Y. Wu, Y. Wang, R. Chen, S. Wang, *Adv. Energy Mater.* **2020**, *10*, 1901227.

[39] J. K. Nørskov, J. Rossmeisl, A. Logadottir, L. Lindqvist, J. R. Kitchin, T. Bligaard, H. Jonsson, *J. Phys. Chem. B* **2004**, *108*, 17886.
[40] B. Hammer, J. K. Nørskov, *Adv. Catal.* **2000**, *45*, 71.
[41] M. T. Greiner, L. Chai, M. G. Helander, W.-M. Tang, Z.-H. Lu, *Adv. Funct. Mater.* **2012**, *22*, 4557.
[42] B. Conway, J. O. M. Bockris, *J. Chem. Phys.* **1957**, *26*, 532.
[43] a) R. Ma, G. Lin, Y. Zhou, Q. Liu, T. Zhang, G. Shan, M. Yang, J. Wang, *npj Comput. Mater.* **2019**, *5*, 78; b) Z. Chen, R. Zheng, M. Graś, W. Wei, G. Lota, H. Chen, B.-J. Ni, *Appl. Catal. B* **2021**, *288*, 120037.
[44] a) J.-P. Sun, Y. Zheng, Z.-S. Zhang, X.-C. Meng, Z.-Z. Li, *Rare Met.* **2024**, *43*, 511; b) Z. Chen, X. Duan, W. Wei, S. Wang, B.-J. Ni, *Nano Energy* **2020**, *78*, 105270; c) G. Liu, Y. Xu, T. Yang, L. Jiang, *Nano Mater. Sci.* **2023**, *5*, 101.
[45] Z. Chen, X. Duan, W. Wei, S. Wang, Z. Zhang, B.-J. Ni, *Nano Res.* **2020**, *13*, 293.
[46] a) Z. Chen, X. Duan, W. Wei, S. Wang, B.-J. Ni, *J. Mater. Chem. A* **2019**, *7*, 14971; b) X. Kang, X.-H. Tan, N. Han, J.-F. Hou, C.-M. Yao, Z.-J. Chen, B.-J. Ni, *Tungsten* **2024**.
[47] K. S. R. Dadallagei, D. L. Parr Iv, J. R. Coduto, A. Lazicki, S. DeBie, C. D. Haas, J. Leddy, *J. Electrochem. Soc.* **2023**, *170*, 086508.
[48] S. A. Shah, L. Xu, R. Sayyar, T. Bian, Z. Liu, A. Yuan, X. Shen, I. Khan, A. A. Tahir, H. Ullah, *Chem. Eng. J.* **2022**, *428*, 132126.
[49] A. Arshad, S. Yun, J. Shi, M. Sun, N. Zafar, A. Hagfeldt, *Chem. Eng. J.* **2022**, *435*, 134913.
[50] M. Tong, L. Wang, P. Yu, C. Tian, X. Liu, W. Zhou, H. Fu, *ACS Sustainable Chem. Eng.* **2018**, *6*, 2474.
[51] a) J. P. Masnica, S. Sibt-e-Hassan, S. Potgieter-Vermaak, Y. N. Regmi, L. A. King, L. Tosheva, *Green Carbon* **2023**, *1*, 160; b) L. Zhao, J. Jiang, S. Xiao, Z. Li, J. Wang, X. Wei, Q. Kong, J. S. Chen, R. Wu, *Nano Mater. Sci.* **2023**, *5*, 329.
[52] M. Li, Y. Wang, Y. Zheng, G. Fu, D. Sun, Y. Li, Y. Tang, T. Ma, *Adv. Energy Mater.* **2020**, *10*, 1903833.
[53] X. Shen, Y. Pan, B. Liu, J. Yang, J. Zeng, Z. Peng, *Phys. Chem. Chem. Phys.* **2017**, *19*, 12628.
[54] a) Y. Lin, Y. Zhu, B. Zhang, Y. A. Kim, M. Endo, D. S. Su, *J. Mater. Chem. A* **2015**, *3*, 21805; b) S. Oh, J. Kim, M. Kim, D. Nam, J. Park, E. Cho, H. Kwon, *J. Mater. Chem. A* **2016**, *4*, 14400; c) H. Shin, N. Kang, D. Kang, J. S. Kang, J. H. Ko, D. H. Lee, S. Park, S. U. Son, Y.-E. Sung, *ChemElectroChem* **2018**, *5*, 1905.
[55] Y. Ha, S. Kang, K. Ham, J. Lee, H. Kim, *J. Phys. Chem. Lett.* **2019**, *10*, 3109.
[56] a) Y.-C. Hsieh, S. D. Senanayake, Y. Zhang, W. Xu, D. E. Polyansky, *ACS Catal.* **2015**, *5*, 5349; b) M. Gattrell, N. Gupta, A. Co, *J. Electroanal. Chem.* **2006**, *594*, 1; c) W. Yang, K. Dastafkan, C. Jia, C. Zhao, *Adv. Mater. Technol.* **2018**, *3*, 1700377.
[57] C. Xi, C. Zou, M. Wang, D. Wu, H. Liu, C. Dong, X.-W. Du, *J. Phys. Chem. C* **2020**, *124*, 5241.
[58] M. Zheng, X. Zhou, Y. Wang, G. Chen, M. Li, *J. Mater. Chem. A* **2023**, *11*, 6591.
[59] Y. Song, W. Xie, M. Shao, X. Duan, *Nano Mater. Sci.* **2023**, *5*, 161.
[60] X. Yang, C. Shang, S. Zhou, J. Zhao, *Nanoscale Horiz.* **2020**, *5*, 1106.
[61] O. Q. Carvalho, R. Marks, H. K. K. Nguyen, M. E. Vitale-Sullivan, S. C. Martinez, L. Árnadóttir, K. A. Stoerzinger, *J. Am. Chem. Soc.* **2022**, *144*, 14809.
[62] L. Fu, J. Zhou, L. Zhou, J. Yang, Z. Liu, K. Wu, H. Zhao, J. Wang, K. Wu, *Chem. Eng. J.* **2021**, *418*, 129422.
[63] T. Erdil, E. Lokcu, I. Yildiz, C. Okuyucu, Y. E. Kalay, C. Toparli, *ACS Omega* **2022**, *7*, 44147.
[64] L. Fu, J. Zhou, Q. Deng, J. Yang, Q. Li, Z. Zhu, K. Wu, *Nanoscale* **2023**, *15*, 677.
[65] B. Wei, Z. Fu, D. Legut, T. C. Germann, S. Du, H. Zhang, J. S. Francisco, R. Zhang, *Adv. Mater.* **2021**, *33*, 2102595.
[66] P. Sivasakthi, M. V. Sangaranarayanan, *New J. Chem.* **2019**, *43*, 8352.
[67] S. Bhardwaj, S. Kapse, S. Dan, R. Thapa, R. S. Dey, *J. Mater. Chem. A* **2023**, *11*, 17045.
[68] Z. Wang, H. Luo, R. Lin, H. Lei, Y. Yuan, Z. Zhu, X. Li, W. Mai, *Appl. Catal. B* **2019**, *257*, 117891.
[69] X. Wang, P. Sun, H. Lu, K. Tang, Q. Li, C. Wang, Z. Mao, T. Ali, C. Yan, *Small* **2019**, *15*, 1804886.
[70] Y. Tong, H. Guo, D. Liu, X. Yan, P. Su, J. Liang, S. Zhou, J. Liu, G. Q. Lu, S. X. Dou, *Angew. Chem., Int. Ed.* **2020**, *59*, 7356.
[71] D. Guan, J. Zhong, H. Xu, Y.-C. Huang, Z. Hu, B. Chen, Y. Zhang, M. Ni, X. Xu, W. Zhou, Z. Shao, *Appl. Phys. Rev.* **2022**, *9*, 011422.
[72] F. Lv, B. Huang, J. Feng, W. Zhang, K. Wang, N. Li, J. Zhou, P. Zhou, W. Yang, Y. Du, D. Su, S. Guo, *Kwansei Gakuin Univ. Nat. Sci. Rev.* **2021**, *8*, nwab019.
[73] L. Zhao, Y. Xiong, X. Wang, R. Zhao, X. Chi, Y. Zhou, H. Wang, Z. Yang, Y.-M. Yan, *Small* **2022**, *18*, 2106939.
[74] X. Luo, R. Jiang, Z. Ma, T. Yang, H. Liu, H. Deng, W. Wu, C. Dong, X.-W. Du, *Phys. Chem. Chem. Phys.* **2022**, *24*, 9188.
[75] S. Chen, C. Wang, F. Gao, Y. Yang, M. Huang, H. Tong, Z. Cheng, P. Wang, P. Wang, J. Tu, X. Zeng, Q. Chen, *J. Mater. Chem. A* **2022**, *10*, 3722.
[76] Y. Da, R. Jiang, Z. Tian, G. Chen, Y. Xiao, J. Zhang, S. Xi, Y. Deng, W. Chen, X. Han, W. Hu, *Adv. Energy Mater.* **2023**, *13*, 2300127.
[77] L. Yang, G. Li, J. Ge, C. Liu, Z. Jin, G. Wang, W. Xing, *J. Mater. Chem. A* **2018**, *6*, 16798.
[78] M. Asadi, K. Kim, C. Liu, A. V. Addepalli, P. Abbasi, P. Yasaei, P. Phillips, A. Behranginia, J. M. Cerrato, R. Haasch, P. Zapol, B. Kumar, R. F. Klie, J. Abiade, L. A. Curtiss, A. Salehi-Khojin, *Science* **2016**, *353*, 467.
[79] Y. Luo, P. Shen, X. Li, Y. Guo, K. Chu, *Chem. Commun.* **2021**, *57*, 9930.
[80] Y. Lin, L. Yang, Y. Zhang, H. Jiang, Z. Xiao, C. Wu, G. Zhang, J. Jiang, L. Song, *Adv. Energy Mater.* **2018**, *8*, 1703623.
[81] M. Zhu, X. Bai, Q. Yan, Y. Yan, K. Zhu, K. Ye, J. Yan, D. Cao, X. Huang, G. Wang, *J. Colloid Interface Sci.* **2021**, *602*, 384.
[82] S. Ji, T. Liu, L. Leng, H. Liu, J. Zhang, M. Zhang, Q. Xu, J. Zhu, M. Qiao, Y. Wang, J. H. Horton, Z. Li, *Appl. Catal. B* **2023**, *320*, 121987.
[83] H. Han, J. Im, M. Lee, D. Choo, *Appl. Catal. B* **2023**, *320*, 121953.
[84] a) F. Kong, X. Cui, Y. Huang, H. Yao, Y. Chen, H. Tian, G. Meng, C. Chen, Z. Chang, J. Shi, *Angew. Chem., Int. Ed.* **2022**, *61*, 202116290; b) Z. Chen, W. Wei, B.-J. Ni, H. Chen, *Environ. Funct. Mater.* **2022**, *1*, 34.
[85] a) H. B. Yang, J. Miao, S.-F. Hung, J. Chen, H. B. Tao, X. Wang, L. Zhang, R. Chen, J. Gao, H. M. Chen, *Sci. Adv.* **2016**, *2*, 1501122; b) J. Hao, Y. Wang, K. Sheng, Z. Tian, Y. Liu, W. Li, J. Li, *Fuel* **2023**, *332*, 126158; c) Z. Chen, R. Zheng, W. Wei, W. Wei, W. Zou, J. Li, B.-J. Ni, H. Chen, *Resour., Conserv. Recycl.* **2022**, *178*, 106037.
[86] S.-H. Kwon, S.-B. Han, D.-H. Kwak, J. Song, K.-W. Park, *J. Ind. Eng. Chem.* **2019**, *80*, 171.
[87] I.-Y. Jeon, H.-J. Noh, J.-B. Baek, *Chem. – An Asian J.* **2020**, *15*, 2282.
[88] Z. Luo, S. Lim, Z. Tian, J. Shang, L. Lai, B. MacDonald, C. Fu, Z. Shen, T. Yu, J. Lin, *J. Mater. Chem.* **2011**, *21*, 8038.
[89] Y. Jia, L. Zhang, L. Zhuang, H. Liu, X. Yan, X. Wang, J. Liu, J. Wang, Y. Zheng, Z. Xiao, E. Taran, J. Chen, D. Yang, Z. Zhu, S. Wang, L. Dai, X. Yao, *Nat. Catal.* **2019**, *2*, 688.
[90] C. Ren, L. Wen, S. Magagula, Q. Jiang, W. Lin, Y. Zhang, Z. Chen, K. Ding, *ChemCatChem* **2020**, *12*, 536.
[91] Q. Li, F. Yuan, C. Yan, J. Zhu, J. Sun, Y. Wang, J. Ren, X. She, *RSC Adv.* **2016**, *6*, 33205.
[92] W. Shen, C. Wang, Q. Xu, H. Liu, Y. Wang, *Adv. Energy Mater.* **2015**, *5*, 1400982.
[93] a) Z. Chen, W. Wei, W. Zou, J. Li, R. Zheng, W. Wei, B.-J. Ni, H. Chen, *Green Chem.* **2022**, *44*, 3208; b) Z. Chen, W. Wei, Y. Shen, B.-J. Ni, *Green Chem.* **2023**, *25*, 5979.

[94] a) Y. H. Li, P. F. Liu, L. F. Pan, H. F. Wang, Z. Z. Yang, L. R. Zheng, P. Hu, H. J. Zhao, L. Gu, H. G. Yang, *Nat. Commun.* **2015**, *6*, 8064; b) Z. Wu, Y. Zhao, W. Jin, B. Jia, J. Wang, T. Ma, *Adv. Funct. Mater.* **2021**, *31*, 2009070.
[95] X. Li, G. Zhang, P. Shen, X. Zhao, K. Chu, *Inorg. Chem. Front.* **2023**, *10*, 280.
[96] X. Zhao, L. Wang, X. Chen, W. Wang, H. L. Xin, X. Du, J. Yang, *J. Power Sources* **2020**, *449*, 227482.
[97] P. Gayen, S. Saha, K. Bhattacharyya, V. K. Ramani, *ACS Catal.* **2020**, *10*, 7734.
[98] Z. Hou, C. Cui, Y. Li, Y. Gao, D. Zhu, Y. Gu, G. Pan, Y. Zhu, T. Zhang, *Adv. Mater.* **2023**, *35*, 2209876.
[99] Y. Wang, X. Li, M. Zhang, Y. Zhou, D. Rao, C. Zhong, J. Zhang, X. Han, W. Hu, Y. Zhang, K. Zaghib, Y. Wang, Y. Deng, *Adv. Mater.* **2020**, *32*, 2000231.
[100] S. K. De, S. Mondal, P. Sen, U. Pal, B. Pathak, k. S. Rawat, M. Bardhan, M. Bhattacharya, B. Satpati, A. De, D. Senapati, *Nanoscale* **2018**, *10*, 11091.
[101] Q. Ma, J. Young, S. Basuray, G. Cheng, J. Gao, N. Yao, W. Zhang, *Nano Today* **2022**, *45*, 101538.
[102] a) Z. Chen, R. Zheng, H. Zou, R. Wang, C. Huang, W. Dai, W. Wei, L. Duan, B.-J. Ni, H. Chen, *Chem. Eng. J.* **2023**, *465*, 142684; b) N. Han, S. Feng, Y. Liang, J. Wang, W. Zhang, X. Guo, Q. Ma, Q. Liu, W. Guo, Z. Zhou, S. Xie, K. Wan, Y. Jiang, A. Vlad, Y. Guo, E. M. Gaigneaux, C. Zhang, J. Fransaer, X. Zhang, *Adv. Funct. Mater.* **2023**, *33*, 2208399; c) Z. Chen, N. Han, W. Wei, D. Chu, B. J. Ni, *EcoEnergy* **2024**, *2*, 114.
[103] a) H. Han, Y.-R. Hong, J. Woo, S. Mhin, K. M. Kim, J. Kwon, H. Choi, Y.-C. Chung, T. Song, *Adv. Energy Mater.* **2019**, *9*, 1803799; b) Y. Guo, R. Zhang, S. Zhang, Y. Zhao, Q. Yang, Z. Huang, B. Dong, C. Zhi, *Energy Environ. Sci.* **2021**, *14*, 3938; c) S. Parmar, T. Das, B. Ray, B. Debnath, S. Gosavi, G. S. Shanker, S. Datar, S. Chakraborty, S. Ogale, *Adv. Energy Sustainability Res.* **2022**, *3*, 2100137.
[104] a) F.-T. Tsai, Y.-Y. Chuang, H.-H. Hsieh, Y.-H. Chen, C.-W. Pao, J.-L. Chen, C.-Y. Lu, C.-K. Hao, W.-F. Liaw, *ACS Appl. Energy Mater.* **2022**, *5*, 5886; b) J. Zhang, L. Ding, W. Sun, W. Bi, Z. Wu, F. Gao, *J. Alloys Compd.* **2021**, *889*, 161770.
[105] Y. Song, M. Sun, S. Zhang, X. Zhang, P. Yi, J. Liu, B. Huang, M. Huang, L. Zhang, *Adv. Funct. Mater.* **2023**, *33*, 2214081.
[106] Y. Zhou, P. Guan, F. Chen, Z. Feng, H. Jia, T. Liang, M. Li, T. Wan, R. Tian, Z. Han, D. Chu, *J. Colloid Interface Sci.* **2023**, *642*, 23.
[107] X. Zhang, T. Liu, T. Guo, Z. Mu, X. Hu, K. He, X. Chen, V. P. Dravid, Z. Wu, D. Wang, *ACS Appl. Mater. Interfaces* **2021**, *13*, 40705.
[108] C. Zhao, J. Long, B. Zhou, R. Zheng, M. He, R. Li, Y. Pan, A. Hu, C. Shu, *J. Mater. Chem. A* **2022**, *10*, 17267.
[109] Y. Zhang, N. Ma, T. Wang, J. Fan, *Nanoscale* **2022**, *14*, 12610.
[110] P. Wang, Y. Zhang, R. Shi, Z. Wang, *New J. Chem.* **2018**, *42*, 19083.
[111] J. Lin, J. Ding, H. Wang, X. Yang, X. Zheng, Z. Huang, W. Song, J. Ding, X. Han, W. Hu, *Adv. Mater.* **2022**, *34*, 2200559.
[112] S. Liu, H. B. Yang, S.-F. Hung, J. Ding, W. Cai, L. Liu, J. Gao, X. Li, X. Ren, Z. Kuang, Y. Huang, T. Zhang, B. Liu, *Angew. Chem., Int. Ed.* **2020**, *59*, 798.
[113] Q. Yu, *Sci. China Mater.* **2023**, *66*, 1079.
[114] C. Guan, R. Ouyang, H. Zhu, Y. Xie, *Electrochim. Acta* **2022**, *427*, 140853.
[115] J. Xiao, M.-R. Gao, S. Liu, J.-L. Luo, *ACS Appl. Mater. Interfaces* **2020**, *12*, 31431.
[116] M. S. Jee, H. Kim, H. S. Jeon, K. H. Chae, J. Cho, B. K. Min, Y. J. Hwang, *Catal. Today* **2017**, *288*, 48.
[117] X. Wu, F. Chen, N. Zhang, A. Qaseem, R. L. Johnston, *Small* **2017**, *13*, 1603876.
[118] Z. Li, D. He, X. Yan, S. Dai, S. Younan, Z. Ke, X. Pan, X. Xiao, H. Wu, J. Gu, *Angew. Chem., Int. Ed.* **2020**, *59*, 18572.
[119] K. Dastafkan, X. Shen, R. K. Hocking, Q. Meyer, C. Zhao, *Nat. Commun.* **2023**, *14*, 547.
[120] S. A. Shah, L. Xu, R. Sayyar, I. Khan, A. Yuan, X. Shen, X. Li, H. Ullah, *Adv. Mater. Interfaces* **2022**, *9*, 2201040.
[121] Y. Li, Y.-Q. Zhu, W. Xin, S. Hong, X. Zhao, H. Yan, S. Xu, *J. Mater. Chem. A* **2021**, *9*, 4176.
[122] C. Zhang, N. Huang, Z. Zhai, L. Liu, B. Chen, B. Yang, X. Jiang, N. Yang, *Adv. Energy Mater.* **2023**, *13*, 2301749.
[123] M. Sharma, J.-H. Jang, D. Y. Shin, J. A. Kwon, D.-H. Lim, D. Choi, H. Sung, J. Jang, S.-Y. Lee, K. Y. Lee, H.-Y. Park, N. Jung, S. J. Yoo, *Energy Environ. Sci.* **2019**, *12*, 2200.
[124] X. Zhao, F. Li, R. Wang, J.-M. Seo, H.-J. Choi, S.-M. Jung, J. Mahmood, I.-Y. Jeon, J.-B. Baek, *Adv. Funct. Mater.* **2017**, *27*, 1605717.
[125] M. Lee, H. S. Jeon, S. Y. Lee, H. Kim, S. J. Sim, Y. J. Hwang, B. K. Min, *J. Mater. Chem. A* **2017**, *5*, 19210.
[126] H. Yang, B. Wang, S. Kou, G. Lu, Z. Liu, *Chem. Eng. J.* **2021**, *425*, 131589.
[127] X. Ji, K. Wang, Y. Zhang, H. Sun, Y. Zhang, T. Ma, Z. Ma, P. Hu, Y. Qiu, *Sustainable Energy Fuels* **2020**, *4*, 407.
[128] M. Wu, J. Zhao, C. Li, R. Liu, *J. Mater. Chem. A* **2022**, *10*, 4791.
[129] W. Chen, W. Wei, F. Li, Y. Wang, M. Liu, S. Dong, J. Cui, Y. Zhang, R. Wang, K. Ostrikov, S.-Q. Zang, *Adv. Funct. Mater.* **2024**, *34*, 2310690.
[130] J.-J. Zhang, H. Su, H.-H. Wang, Z.-H. Xue, B. Zhang, X. Wei, X.-H. Li, S.-I. Hirano, J.-S. Chen, *Nano Energy* **2017**, *39*, 321.
[131] K. He, T. Tadesse Tsega, X. Liu, J. Zai, X.-H. Li, X. Liu, W. Li, N. Ali, X. Qian, *Angew. Chem., Int. Ed.* **2019**, *58*, 11903.
[132] X. H. Chen, J. Y. Ren, N. B. Li, H. Q. Luo, *J. Colloid Interface Sci.* **2023**, *651*, 760.
[133] M. Gu, L. Jiang, S. Zhao, H. Wang, M. Lin, X. Deng, X. Huang, A. Gao, X. Liu, P. Sun, X. Zhang, *ACS Nano* **2022**, *16*, 15425.
[134] J. Yao, M. Zhang, X. Ma, L. Xu, F. Gao, J. Xiao, H. Gao, *J. Colloid Interface Sci.* **2022**, *607*, 1343.
[135] J. Zhang, H. Yu, J. Yang, X. Zhu, M. Hu, J. Yang, *J. Alloys Compd.* **2022**, *924*, 166613.
[136] J. Sun, H. Xue, J. Sun, N. Guo, T. Song, Y.-R. Hao, Q. Wang, *Chin. Chem. Lett.* **2024**, *35*, 109002.
[137] J. Liu, L. He, S. Zhao, L. Hu, S. Li, Z. Zhang, M. Du, *Small* **2023**, *19*, 2302600.
[138] S. Zhang, C. Tan, R. Yan, X. Zou, F.-L. Hu, Y. Mi, C. Yan, S. Zhao, *Angew. Chem., Int. Ed.* **2023**, *62*, 202302795.
[139] Z. Zhuang, L. Xia, J. Huang, P. Zhu, Y. Li, C. Ye, M. Xia, R. Yu, Z. Lang, J. Zhu, L. Zheng, Y. Wang, T. Zhai, Y. Zhao, S. Wei, J. Li, D. Wang, Y. Li, *Angew. Chem., Int. Ed.* **2023**, *62*, 202212335.
[140] C. Mu, H. Xin, Q. Luo, Y. Li, F. Ma, *J. Mater. Chem. A* **2023**, *11*, 7016.
[141] Q. Zhou, L. Liao, Q. Bian, F. Yu, D. Li, J. Zeng, L. Zhang, H. Wang, D. Tang, H. Zhou, Z. Ren, *Small* **2022**, *18*, 2105642.
[142] C. Pi, X. Li, X. Zhang, H. Song, Y. Zheng, B. Gao, A. Kızılaslan, P. K. Chu, K. Huo, *Small* **2022**, *18*, 2201137.
[143] X. Wang, X. Liu, C.-J. Tong, X. Yuan, W. Dong, T. Lin, L.-M. Liu, F. Huang, *J. Mater. Chem. A* **2016**, *4*, 7762.
[144] Y. Li, W. Niu, T. Chen, Y. Sun, M. Yu, *Appl. Catal. B* **2023**, *321*, 122037.
[145] G. Song, S. Luo, Q. Zhou, J. Zou, Y. Lin, L. Wang, G. Li, A. Meng, Z. Li, *J. Mater. Chem. A* **2022**, *10*, 18877.
[146] a) A. Kagkoura, H. J. Ojeda-Galván, M. Quintana, N. Tagmatarchis, *Small* **2023**, *19*, 2208285; b) S. Zhu, L. Ding, X. Zhang, K. Wang, X. Wang, F. Yang, G. Han, *Angew. Chem., Int. Ed.* **2023**, *62*, 202309545; c) C. Cheng, W. Ao, H. Ren, Z. Fan, T. Xu, L. Dai, P. Yin, *Sci. China Mater.* **2023**, *66*, 1383; d) X. Xiao, Z. Li, Y. Xiong, Y.-W. Yang, *J. Am. Chem. Soc.* **2023**, *145*, 16548.
[147] W. Zhan, H. Wang, J. Gao, X. Tang, X. Zhu, Y. Xiao, X. Sun, W. Gao, H. Yin, *Small Struct.* **2023**, *4*, 2300167.
[148] C. Liu, F. Liu, H. Li, J. Chen, J. Fei, Z. Yu, Z. Yuan, C. Wang, H. Zheng, Z. Liu, M. Xu, G. Henkelman, L. Wei, Y. Chen, *ACS Nano* **2021**, *15*, 3309.

[149] a) G. Chen, C. Zhang, S. Xue, J. Liu, Y. Wang, Y. Zhao, K. Pei, X. Yu, R. Che, *Small* **2021**, *17*, 2100510; b) X.-X. Li, X.-C. Liu, C. Liu, J.-M. Zeng, X.-P. Qi, *Tungsten* **2023**, *5*, 100.
[150] W. Duan, G. Li, Z. Lei, T. Zhu, Y. Xue, C. Wei, C. Feng, *Water Res.* **2019**, *161*, 126.
[151] A. S. Haile, H. A. Hansen, W. Yohannes, Y. S. Mekonnen, *J. Phys. Chem. Lett.* **2021**, *12*, 3552.
[152] G. Lin, Q. Ju, Y. Jin, X. Qi, W. Liu, F. Huang, J. Wang, *Adv. Energy Mater.* **2021**, *11*, 2101050.
[153] a) Z. Zhao, Z. Yi, Y. Duan, R. Pathak, X. Cheng, Y. Wang, J. W. Elam, X. Wang, *Chem. Eng. J.* **2023**, *463*, 142397; b) C. Fan, X. Wu, M. Li, X. Wang, Y. Zhu, G. Fu, T. Ma, Y. Tang, *Chem. Eng. J.* **2022**, *431*, 133829; c) Z. Chen, R. Zheng, S. Deng, W. Wei, W. Wei, B.-J. Ni, H. Chen, *J. Mater. Chem. A* **2021**, *9*, 25032; d) Z. Chen, X. Duan, W. Wei, S. Wang, B.-J. Ni, *Nano Energy* **2020**, *78*, 105392.
[154] B. Zhang, H. Liu, P. Zhai, R. Zhang, W. Wang, P. Khangale, D. Hildebrandt, X. Liu, S. Qiao, *Adv. Funct. Mater.* **2023**, *33*, 2211440.
[155] Y. Liu, H. Zhang, W. Song, Y. Zhang, Z. Hou, G. Zhou, Z. Zhang, J. Liu, *Chem. Eng. J.* **2023**, *451*, 138905.
[156] Z.-H. Xue, H. Su, Q.-Y. Yu, B. Zhang, H.-H. Wang, X.-H. Li, J.-S. Chen, *Adv. Energy Mater.* **2017**, *7*, 1602355.
[157] C. Gu, G. Zhou, J. Yang, H. Pang, M. Zhang, Q. Zhao, X. Gu, S. Tian, J. Zhang, L. Xu, Y. Tang, *Chem. Eng. J.* **2022**, *443*, 136321.
[158] C. Wu, G. Qi, J. Zhang, J. Cheng, B. Wang, *Small* **2023**, *19*, 2302078.
[159] X. Fan, D. Zhao, Z. Deng, L. Zhang, J. Li, Z. Li, S. Sun, Y. Luo, D. Zheng, Y. Wang, B. Ying, J. Zhang, A. A. Alshehri, Y. Lin, C. Tang, X. Sun, Y. Zheng, *Small* **2023**, *19*, 2208036.
[160] Z. Li, S. Xu, Y. Shi, X. Zou, H. Wu, S. Lin, *Chem. Eng. J.* **2021**, *414*, 128814.
[161] a) Y. Feng, Y. Guan, E. Zhou, X. Zhang, Y. Wang, *Adv. Sci.* **2022**, *9*, 2201339; b) B. Zhu, L. Fan, N. Mushtaq, R. Raza, M. Sajid, Y. Wu, W. Lin, J.-S. Kim, P. D. Lund, S. Yun, *Electrochem. Energy Rev.* **2022**, *4*, 757; c) X. Lv, Z. Xiao, H. Wang, X. Wang, L. Shan, F. Wang, C. Wei, X. Tang, Y. Chen, *J. Energy Chem.* **2021**, *54*, 626.
[162] a) Q. Ouyang, S. Cheng, C. Yang, Z. Lei, *J. Mater. Chem. A* **2022**, *10*, 11938; b) Y. Zhang, P. Guo, S. Niu, J. Wu, W. Wang, B. Song, X. Wang, Z. Jiang, P. Xu, *Small Methods* **2022**, *6*, 2200084.
[163] Y. Zeng, Z. Cao, J. Liao, H. Liang, B. Wei, X. Xu, H. Xu, J. Zheng, W. Zhu, L. Cavallo, Z. Wang, *Appl. Catal. B* **2021**, *292*, 120160.
[164] a) C. Feng, W. Zhou, H. Wu, Q. Huo, J. Shao, X. Li, H. Yang, Q. Hu, C. He, *Appl. Catal. B* **2024**, *341*, 123280; b) Q. Zhou, G. Song, J. Zou, S. Luo, A. Meng, Z. Li, *Int. J. Hydrogen Energy* **2023**, *48*, 15921.
[165] J. Li, Y. Tan, M. Zhang, W. Gou, S. Zhang, Y. Ma, J. Hu, Y. Qu, *ACS Energy Lett.* **2022**, *7*, 1330.
[166] J. Li, J. Hu, M. Zhang, W. Gou, S. Zhang, Z. Chen, Y. Qu, Y. Ma, *Nat. Commun.* **2021**, *12*, 3502.
[167] a) Z. Ren, S. Wang, J. Yu, F. Mao, K. Wang, H. Wu, *Chem. Eng. J.* **2023**, *470*, 144107; b) Z. Cheng, Y. Xiao, W. Wu, X. Zhang, Q. Fu, Y. Zhao, L. Qu, *ACS Nano* **2021**, *15*, 11417; c) Z. Liu, K. Wang, Y. Li, S. Yuan, G. Huang, X. Li, N. Li, *Appl. Catal. B* **2022**, *300*, 120696.
[168] Y. Jiang, H. Liu, Y. Jiang, Y. Mao, W. Shen, M. Li, R. He, *Appl. Catal. B* **2023**, *324*, 122294.
[169] Z.-L. Liu, X. Wu, Y. Shao, J. Qi, Y. Cao, L. Huang, C. Liu, J.-O. Wang, Q. Zheng, Z.-L. Zhu, K. Ibrahim, Y.-L. Wang, H.-J. Gao, *Sci. Bull.* **2018**, *63*, 419.

Zhijie Chen received his Ph.D. degree in environmental engineering from the University of Technology Sydney (Australia) in 2022. He now works as a Postdoc researcher at the University of New South Wales, Sydney. His research mainly work focuses on developing green techniques and cost-effective functional materials for sustainable energy and environmental applications, such as (waste)water electrolysis, plastic waste upcycling, and wastewater remediation.

Tianyi Ma received his Ph.D. in physical chemistry in 2013 from Nankai University, China. He is a Fellow of the Royal Society of Chemistry and Clarivate's Global Highly Cited Researcher. He was awarded an Australian Research Council Discovery Early Career Researcher Award (2014) and Future Fellowship (2021). He is currently a full professor at RMIT University, focusing on functional photocatalytic, electrocatalytic, thermocatalytic, and piezocatalytic materials for renewable solar, mechanical, and thermal energy harvesting and utilization, as well as carbon capture, utilization, and storage; these processes are further incorporated into his developed next-generation high-performance battery and supercapacitor-based energy storage devices.

Wei Wei obtained her Ph.D. degree in Environmental Science and Engineering from Harbin Institute of Technology (China) in 2018 and awarded an Outstanding PhD Award from Chinese Education Department. She joined the University of Technology Sydney in 2019, and currently is an Australian Research Council (ARC) DECRA Fellow and Lecturer at the School of Civil and Environmental Engineering of UTS. Her research focuses on the development and application of innovative and sustainable techniques to achieve sustainable energy recovery from waste.

Wai-Yeung Wong received his Ph.D. degree from The University of Hong Kong SAR, China (1995). He is currently the Chair Professor of Chemical Technology, Clarea Au Professor in Energy and Dean of Faculty of Science at The Hong Kong Polytechnic University. He is the President of the Hong Kong SAR, China Chemical Society. He is also the recipient of the RSC Chemistry of the Transition Metals Award, State Natural Science Award (Second-Class) from China, and RGC Senior Research Fellow Award from Hong Kong SAR, China. His research interest focuses on the design of functional materials for advanced energy applications.

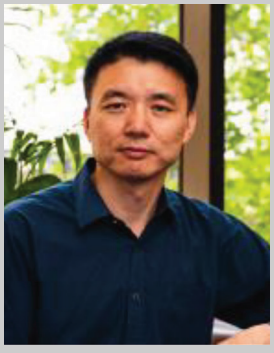

Chuan Zhao received his Ph.D. degree (2002) from Northwest University. He then completed postdoctoral research at the University of Oldenburg and Monash University before starting his independent research career at the University of New South Wales, Sydney. He was awarded the prestigious Australian Research Fellow (2011), Future Fellow (2017), and R.H. Stodkes Medal from the Royal Australian Chemical Insititute (RACI) in 2023. He has been elected Fellows of RACI, Royal Society of Chemistry, and Royal Society of New South Wales. His research focuses on discovering novel electrochemical methods and materials for water splitting, hydrogen fuel cells, CO_2 and N_2 reduction, aqueous batteries, and sensors.

Bing-Jie Ni received his Ph.D. degree in environmental engineering in June 2009. He currently is a full professor at the University of New South Wales, Sydney. He is a Fellow of the Royal Society of Chemistry and Clarivate Global Highly Cited Researcher. His work focuses on the integration of different disciplines to develop innovative and sustainable technological solutions to achieve environmental and energy sustainability.